Facioscapulohumeral Muscular Dystrophy is Associated With Altered Myoblast Proteome Dynamics

Authors

Yusuke Nishimura, Adam J. Bittel, Connor A. Stead, Yi-Wen Chen, and Jatin G. Burniston

Correspondence

ychen@childrensnational.org; j.burniston@ljmu.ac.uk

In Brief

Nishimura *et al.* used dynamic proteome profiling to uncover new disease mechanisms underpinned by post-transcriptional processes in FSHD. Deuterium oxide (D_2O) labeling and peptide mass spectrometry were used to obtain the abundance and turnover rates of proteins in myoblasts from two individuals with FSHD and their unaffected siblings. The results identified that FSHD myoblasts exhibit greater abundance but a slower turnover rate of mitochondrial proteins, which may indicate an accumulation of "older" less viable mitochondrial proteins in FSHD myoblasts.

Graphical Abstract

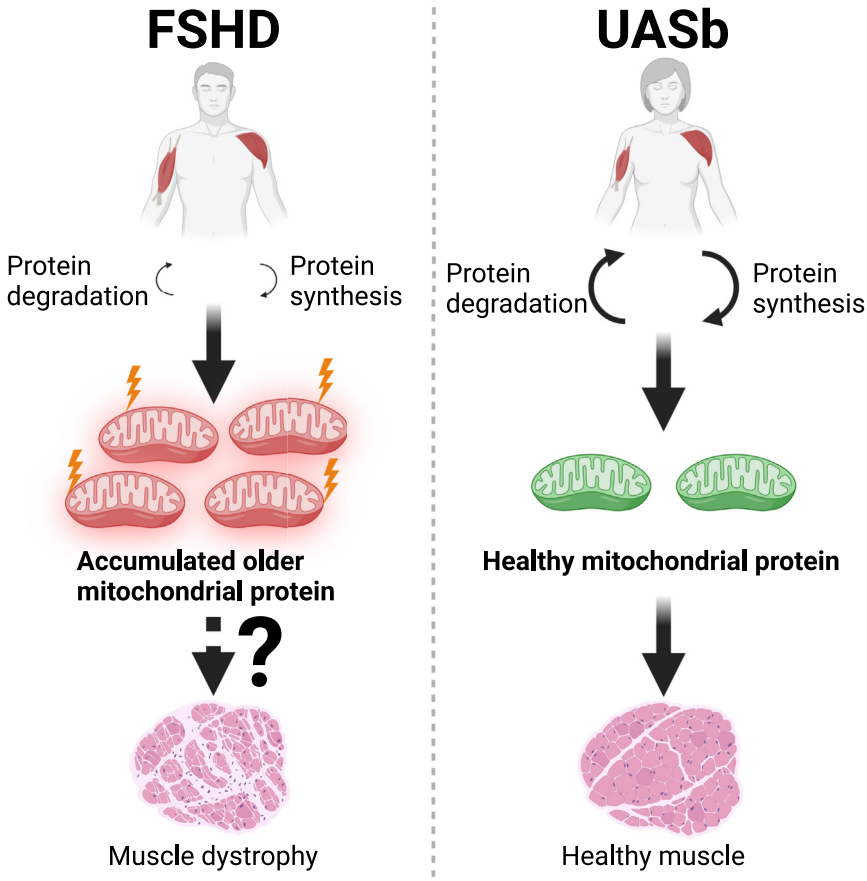

Highlights

- Dynamic profiling of myoblasts from FSHD patients and their unaffected siblings.
- Median protein turnover is slower in FSHD myoblasts than their unaffected siblings.
- Mitochondrial proteins are more abundant in FSHD myoblasts.
- Mitochondrial proteins exhibit a slower protein turnover rate in FSHD myoblasts.
- 2′-MOE treatment partly reversed the dysregulation of mitochondrial proteins in FSHD.

2023, Mol Cell Proteomics *22*(*8*), 100605

https://doi.org/10.1016/j.mcpro.2023.100605

Facioscapulohumeral Muscular Dystrophy is Associated With Altered Myoblast Proteome Dynamics

Yusuke Nishimura[1,‡], Adam J. Bittel[2,‡], Connor A. Stead[1], Yi-Wen Chen[2,*§], and Jatin G. Burniston[1,*§]

Proteomic studies in facioscapulohumeral muscular dystrophy (FSHD) could offer new insight into disease mechanisms underpinned by post-transcriptional processes. We used stable isotope (deuterium oxide; D_2O) labeling and peptide mass spectrometry to investigate the abundance and turnover rates of proteins in cultured muscle cells from two individuals affected by FSHD and their unaffected siblings (UASb). We measured the abundance of 4420 proteins and the turnover rate of 2324 proteins in each (n = 4) myoblast sample. FSHD myoblasts exhibited a greater abundance but slower turnover rate of subunits of mitochondrial respiratory complexes and mitochondrial ribosomal proteins, which may indicate an accumulation of "older" less viable mitochondrial proteins in myoblasts from individuals affected by FSHD. Treatment with a 2′-O-methoxyethyl modified antisense oligonucleotide targeting exon 3 of the double homeobox 4 (DUX4) transcript tended to reverse mitochondrial protein dysregulation in FSHD myoblasts, indicating the effect on mitochondrial proteins may be a DUX4-dependent mechanism. Our results highlight the importance of post-transcriptional processes and protein turnover in FSHD pathology and provide a resource for the FSHD research community to explore this burgeoning aspect of FSHD.

Facioscapulohumeral muscular dystrophy (FSHD) is the third most common muscular dystrophy and has a prevalence of approximately 1:20,000. Currently, there is no effective treatment or cure for FSHD, which is marked by gradual loss of muscle mass and function and eventual loss of independence (1). Ectopic expression of the double homeobox 4 (*DUX4*) gene is the key molecular cause of the primary (95% of cases) disease phenotype FSHD1 (OMIM 158900) and less common FSHD2 (OMIM 158901) (2). DUX4 instigates widespread changes in muscle gene expression (3), including aberrant activation of other transcription factors. Several biological processes are known to be disrupted by DUX4 expression in muscle, including myogenic differentiation and cell cycle (4), oxidative stress sensitivity (5), DNA damage (6), Wnt/β-catenin signaling (7), metabolic stress and mitochondrial dysfunction (8), and p53-mediated apoptosis (9). However, the mechanisms that connect DUX4 expression to muscle toxicity are not yet fully understood despite extensive studies on gene regulation and transcriptional processes (4, 10–12).

Proteomic studies in FSHD are currently scarce but have the potential to bring new insight into the role of post-transcriptional processes in FSHD and help connect the dysregulation of gene programs with cellular abnormalities. However, Jagannathan *et al.* (13) reported a striking disconnection between changes in gene expression and changes in the abundance of the corresponding proteins when DUX4 is artificially expressed in immortalized MB135 human myoblasts. After induction of DUX4, there was a greater than a 4-fold change in the abundance of 208 out of 4005 proteins studied, but when proteomic data were aligned with earlier gene expression data (14), one-third of changes in protein abundance were not matched by a change in gene expression or the change in expression of the gene was diametrically opposite to the change in protein abundance (13). This disconnection between mRNA and protein responses to DUX4 expression could occur, for example, through (mis)-regulation of synthetic processes, degradative processes, or a combination of the two. Artificial expression of DUX4 results in a 50% reduction in bulk protein synthesis measured by ^{35}S-methionine incorporation in M135 myoblasts (13). However, it is not clear whether similar disruptions in protein turnover occur in patient-derived samples, and the measurement of the "bulk" synthesis rate of protein mixtures (13) cannot distinguish individual protein responses. The aforementioned 50% reduction

From the [1]Research Institute for Sport & Exercise Sciences, Liverpool John Moores University, Liverpool, United Kingdom; [2]Center for Genetic Medicine Research, Children's National Medical Center, Washington, District of Columbia, USA
‡These authors were joint first authors.
§These authors were joint senior authors.
*For correspondence: Yi-Wen Chen, ychen@childrensnational.org; Jatin G. Burniston, j.burniston@ljmu.ac.uk.

https://doi.org/10.1016/j.mcpro.2023.100605

in ^{35}S-methionine incorporation could represent a blanket 50% reduction in the synthesis of all proteins or complete inhibition in the synthesis of 50% of proteins. In addition, DUX4 target genes that were faithfully translated into functional proteins included several known or putative E3 ubiquitin ligases that could dysregulate protein degradation (13).

DUX4 overexpression in a myoblast cell line (13, 15) is an optimized research model and may not faithfully reflect FSHD pathophysiology, where DUX4 expression is transient and often localized to small numbers of myonuclei at a particular time. Other proteomic analyses (16, 17) have used muscle samples of individuals with FSHD, including non-clinically affected muscles to focus on the fundamental pathophysiological mechanisms of FSHD while minimizing the impact of dystrophic processes. In addition, myotubes (18) or myoblasts (19) and interstitial fluid samples (20) from individuals with FSHD and their unaffected siblings (UASb) have been studied using proteomic techniques. Herein, we performed proteomic analysis on previously generated and validated (21) immortalized myoblasts from matched pairs of individuals with FSHD and UASb. To the best of our knowledge, the present work represents the first proteomic analysis of immortalized FSHD and UASb cell lines reported in Homma *et al.* (21), which have been characterized across several previous studies (8, 10, 22–26).

To study protein turnover, myoblasts were cultured with the stable isotope, deuterium oxide (D_2O), which labels amino acid precursors and enables the fraction of newly synthesized protein to be calculated from time-dependent differences in the mass isotopomer distribution of peptide mass spectra (27, 28). Using this proteomics approach, we surveyed the abundances and turnover rates of thousands of proteins in FSHD and UASb cell cultures and discovered some proteins exhibit discordance between differences in abundance and turnover rate.

EXPERIMENTAL PROCEDURES

Cell Culture and Deuterium Oxide Labeling

Immortalized human myoblasts from individuals with FSHD and their UASb were obtained from the Senator Paul D. Wellstone Muscular Dystrophy Cooperative Research Center for FSHD at the University of Massachusetts Chan Medical School (Worcester, MA, USA) and Dr Woodring E Wright at the University of Texas Southwestern Medical Center. The collection of muscle biopsies, isolation of myoblast and purification, and molecular characterization of FSHD and UASb cells were originally described by Homma *et al.* (21).

An overview of the study design is shown in Figure 1*A* and characteristics of FSHD and UASb donors are presented in Figure 1*B*. Consistent with a previous work by Pandey *et al.* (29), immortalized FSHD myoblasts were cultured in LHCN medium (4:1 DMEM:Medium 199 (ThermoFisher Scientific, Waltham, MA, USA) supplemented with 15% fetal bovine serum (FBS, Hyclone, South Logan), 0.03 mg/ml ZnSO4 (Sigma), 1.4 mg/ml Vitamin B12 (Sigma-Aldrich), 2.5 ng/ml hepatocyte growth factor (Chemicon International), 10 ng/ml basic fibroblast growth factor (Millipore), and 0.02 M HEPES (Life Technologies) with dexamethasone (140 nmol/ml) to suppress DUX4 expression and facilitate the proliferation of FSHD cells. After attaining 80% confluency, cultures were switched to LHCN media without dexamethasone (LHCN-DEX) for 3 days to wean myoblasts from the effects of dexamethasone. Myoblasts were then cultured for an additional 24 h in LHCN -DEX media supplemented with 4% (v/v) deuterium oxide (D_2O) to label newly synthesized proteins and then harvested for analysis. Myoblasts derived from UASb were treated identically to provide a control group at each experimental time point.

In a separate experiment (reported in Figure 6) myoblasts were initially cultured as shown in Figure 1*A* and were then cultured with 4% (v/v) D_2O with or without 1uM of 2′-O-methoxyethyl (2′-MOE) modified antisense oligonucleotide targeting exon three of the DUX4 transcript, as previously described (30), for 24 h and harvested for analysis. For the MOE (–) condition, the same volume of water as treated in 2′-MOE condition was added as a vehicle control.

Protein Extraction and Quantification

Following treatments and timings detailed above, the medium was aspirated, and the cell monolayer was washed twice with ice-cold PBS. Cells were lysed with 250 μl of Urea buffer (8 M Urea, 100 mM Tris, pH ~ 8.5) for 5 min at room temperature, scraped into Eppendorf tubes in preparation for total protein quantification, digestion, and proteomic analyses. Total protein concentration (μg/μl) was quantified against bovine serum albumin (BSA) standards using the Pierce BCA Protein Assay Kit (Rockford, IL, USA), according to the manufacturer's instructions.

Protein Digestion

Filter-Aided Sample Preparation (FASP) was performed using lysates containing 100 μg protein and incubated at 37 °C for 15 min in UA buffer with 100 mM dithiothreitol followed by 20 min at 4 °C in UA buffer containing 50 mM iodoacetamide (protected from light). Samples were washed twice with 100 μl UA buffer and transferred to 50 mM ammonium hydrogen bicarbonate (Ambic). Sequencing grade trypsin (Promega) in 50 mM Ambic was added at an enzyme to protein ratio of 1:50 and the samples were digested overnight at 37 °C. Peptides were collected in 50 mM Ambic and trifluoracetic acid (TFA) was added to a final concentration of 0.2% (v/v) to terminate digestion. Aliquots, containing 4 μg peptides, were desalted using C18 Ziptips (Millipore) and eluted in 50:50 of acetonitrile and 0.1% TFA. Peptide solutions were dried by vacuum centrifugation for 25 min at 60 °C and peptides were resuspended in 0.1% formic acid spiked with 10 fmol/ul yeast ADH1 (MassPrep standard; Waters Corp) in preparation for LC-MS/MS analysis.

Liquid Chromatography-Mass Spectrometry Analysis

Data reported in Figures 1–5 were generated from the analysis of peptide mixtures using an Ultimate 3000 RSLC nano liquid chromatography system (Thermo Scientific) coupled to a Fusion mass spectrometer (Thermo Scientific). Samples were loaded onto the trapping column (Thermo Scientific, PepMap100, C18, 75 μm × 20 mm), using partial loop injection, for 7 min at a flow rate of 9 μl/min with 0.1% (v/v) TFA. Samples were resolved on a 500 mm analytical column (Easy-Spray C18 75 μm, 2 μm column) using a gradient of 96.2% A (0.1% formic acid) 3.8% B (79.9% ACN, 20% water, 0.1% formic acid) to 50% A 50% B over 90 min at a flow rate of 300 nl/min. The data-dependent program used for data acquisition consisted of a 120,000-resolution full-scan MS scan (AGC set to 4e5 ions with a maximum fill time of 50 ms) with MS/MS using quadrupole ion selection with a 1.6 m/z window, HCD fragmentation with a normalized collision energy of 32 and LTQ analysis using the rapid scan setting and a maximum fill time of 35 ms. The machine was set to perform as many MS/MS scans as possible to maintain a cycle time of 0.6 s. To

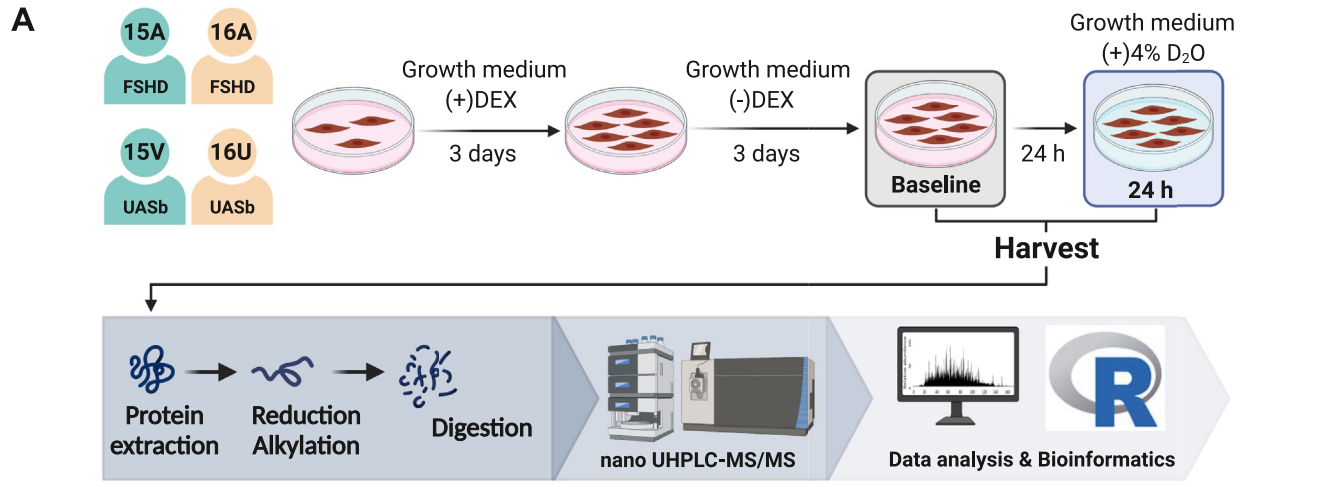

B

Participant	Sex (Age)	Fragment size (Repeat Units)	Strength (De/Bi)
15A FSHD1	M (67)	28 / >112 (8 / 34+)	5 / 5 4+ / 5
15V Sister of 15A	F (60)	107 / >112 (32 / 34+)	5 / 5 5 / 5
16A FSHD1	F (56)	20 / >97 (6 / 29-30)	5- / 5 4+ / 5
16U Sister of 16A	F (60)	59 / 93 / 97 (17 / 28 /29)	5 / 5 5 / 5

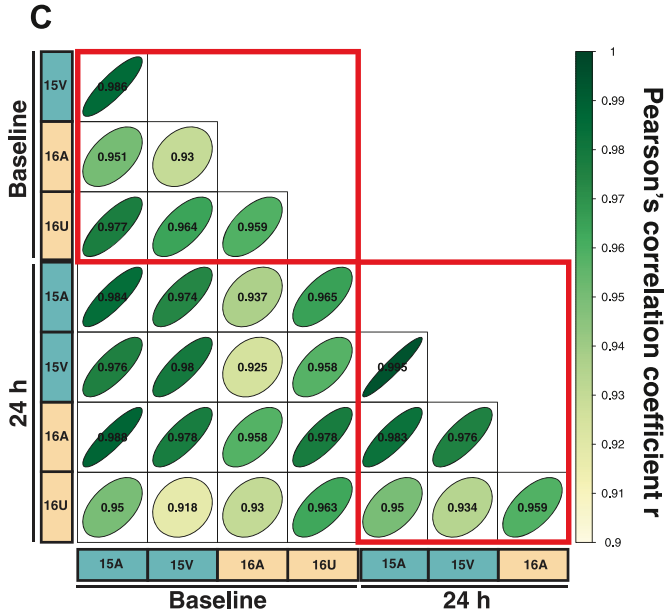

FIG. 1. **Dynamic proteome profiling of two pairs of FSHD and UASb myoblasts.** *A*, experimental design and workflow for sample preparation and analysis. *B*, characteristics of FSHD and UASb donors, including shortened length of the 4q D4Z4 repeat array (*bold red*) and muscle score using the Medical Research Council (MRC) scale where 5/5 is maximum strength. Data were retrieved from Homma *et al.* (21). *C*, matrix correlation of abundance data, n = 4420 proteins, using Pearson's correlation coefficient. Bi, biceps; Del, deltoid.

avoid repeated selection of peptides for MS/MS, the program used a 60-s dynamic exclusion window.

Data reported in Figure 6 were generated from the analysis of peptide mixtures using an Ultimate 3000 RSLC nano liquid chromatography system (Thermo Scientific) coupled to Q-Exactive orbitrap mass spectrometer (Thermo Scientific). Samples were loaded on to the trapping column (Thermo Scientific, PepMap NEO, 5 µm C18, 300 µm × 5 mm), using ulPickUp injection, for 1 min at a flow rate of 25 µl/min with 0.1% (v/v) TFA and 2% (v/v) ACN. Samples were resolved on a 750 mm analytical column (Easy-Spray C18 75 µm, 2 µm column) using a gradient of 97.5% A (0.1% formic acid) 2.5% B (79.9% ACN, 20% water, 0.1% formic acid) to 50% A 50% B over 150 min at a flow rate of 250 nl/min. The data-dependent selection of the top-ten precursors selected from a mass range of m/z 300 to 1600 consisted of a 70,000-resolution (at m/z 200) MS scan (AGC set to 3^{e6} ions with a maximum fill time of 240 ms). MS/MS data were acquired using quadrupole ion selection with a 3.0 m/z window, HCD fragmentation with a normalized collision energy of 30, and orbitrap analyzer at 17,500 resolution at m/z 200 (AGC target 5^{e4} ion with a maximum fill time of 80 ms). To avoid repeated selection of peptides for MS/MS, the program used a 30-s dynamic exclusion window.

Label-Free Quantitation of Protein Abundances

Progenesis Quantitative Informatics for Proteomics (QI-P; Nonlinear Dynamics, Waters Corp, Version 4.2) was used for label-free quantitation, consistent with previous studies (31–34). Log-transformed MS data were normalized by inter-sample abundance ratio, and relative protein abundances were calculated using nonconflicting peptides only. In addition, abundance data were normalized to the three most abundant peptides of yeast ADH1 to obtain abundance estimates

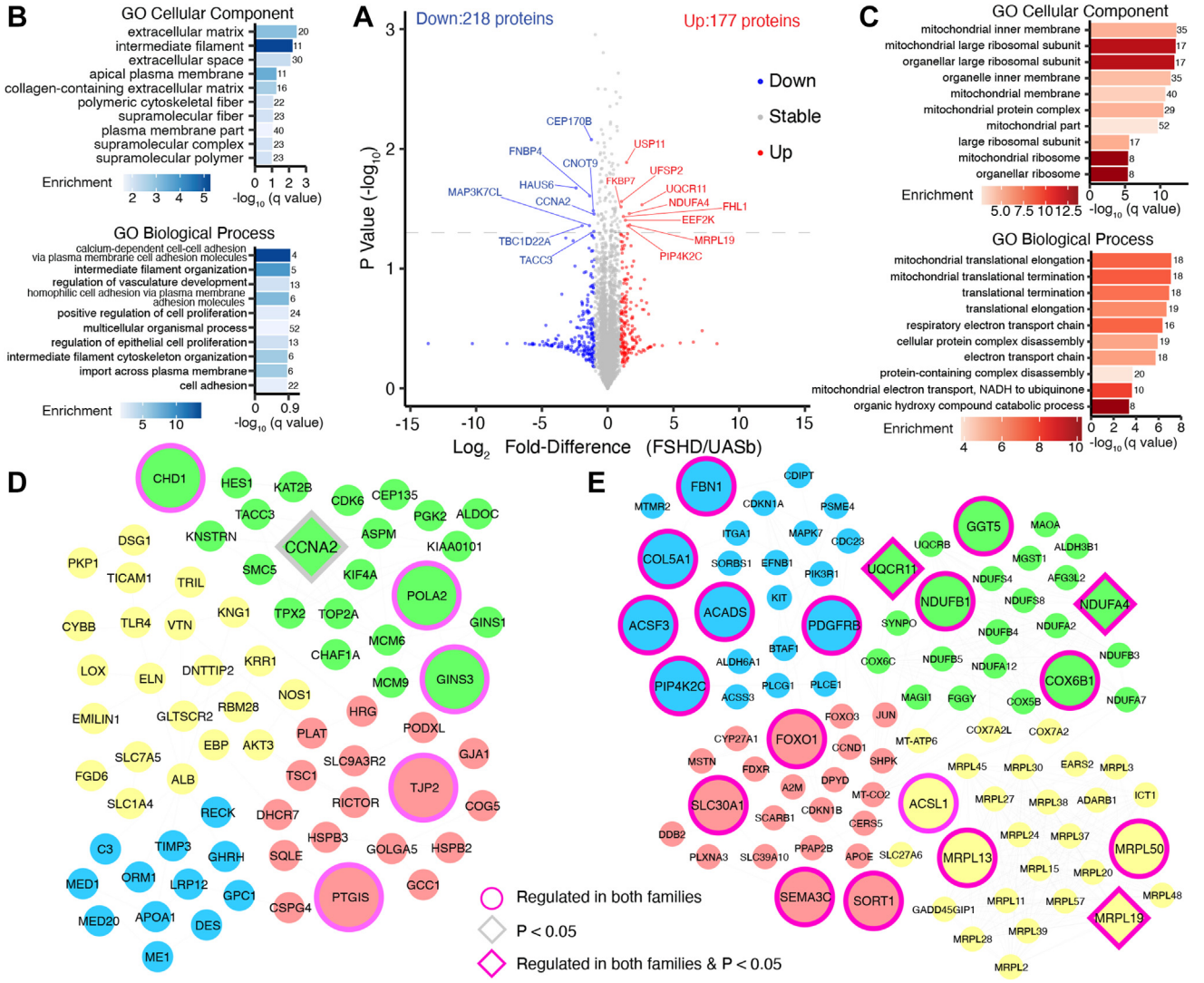

FIG. 2. **Differences in protein abundance between FSHD and UASb myoblasts.** *A*, volcano plot comparing the Log_2 Fold-Difference (FSHD/UASb) protein abundance plotted against the $-Log_{10}$ *p* value (n = 4420). Colored data points represent proteins more abundant (*red*, log_2 Diff. > 1), less abundant (*blue*, log_2 Diff. < –1), or stable (*grey*, log_2 Diff. < 1 and > –1) in FSHD compared to UASb myoblasts. The *dashed horizontal line* shows a threshold of statistical significance ($p < 0.05$). Gene ontology (GO) analysis of cellular component and biological process in proteins (*B*) depleted (log_2 Diff. < –1) or (*C*) enriched (log_2 Diff. > 1) in FSHD compared to UASb myoblasts. GO terms were ranked by $-log_{10}$ (q value) and the number of proteins included in each GO term reported alongside each entry. Each bar chart colour scale represents the level of GO enrichment. STRING protein interaction network for proteins (*D*) depleted (log_2 Diff. < –1) or (*E*) enriched (log_2 Diff. > 1) in FSHD compared to UASb myoblasts. The STRING interaction network was generated using a minimum interaction score of 0.7 and the interaction network was clustered using k-means clustering. Proteins without interaction partners were omitted from visualization.

(ABD_{mol}) in fmol/µg protein. MS/MS spectra were exported in Mascot generic format and searched against the Swiss-Prot database (2021_03) restricted to Homo-sapiens (20,371 sequences) using a locally implemented Mascot server (v.2.2.03; www.matrixscience.com). The enzyme specificity was trypsin with two allowed missed cleavages, carbamidomethylation of cysteine (fixed modification), deamidation of asparagine and glutamine (variable modification), and oxidation of methionine (variable modification). MS data were searched with *m/z* error tolerances of 10 ppm for peptide ions and either 0.6 Da (FUSION data) or 20 ppm (Q-Exactive data) for fragment ion spectra. Peptide results were filtered to 1% FDR based on decoy search and at least one unique peptide was required to identify each protein. The Mascot output (xml format), restricted to non-homologous protein identifications was recombined with MS profile data in Progenesis.

Measurement of Protein Turnover Rates

Protein fractional turnover rates (FTR) were calculated consistently with our previous work (33). Mass isotopomer abundance data were extracted from MS spectra using Progenesis QI (Nonlinear Dynamics; Waters Corp). The abundance of m_0–m_3 mass isotopomers was collected over the entire chromatographic peak for nonconflicting peptides that were used for label-free

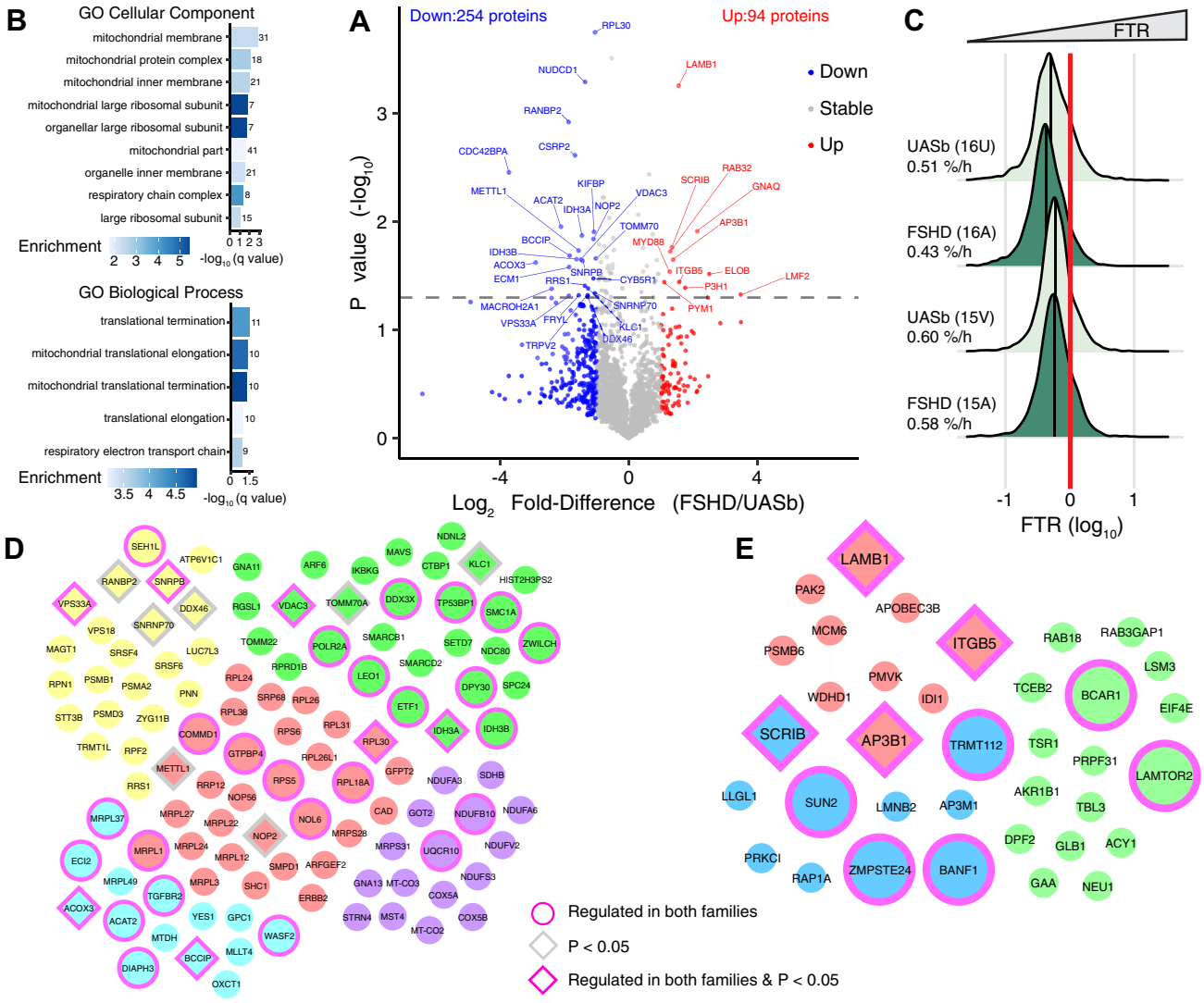

FIG. 3. **Differences in protein turnover rate between FSHD and UASb myoblasts.** *A*, volcano plot comparing the Log_2 fold-difference (FSHD/UASb) in protein turnover plotted against the $-Log_{10}$ *p* value (n = 2324 proteins). Colored data points represent proteins with greater (*red*, log_2 Diff. > 1), lesser (*blue*, log_2 Diff. < −1), or stable (*grey*, log_2 Diff. < 1 and > −1) rates of turnover in FSHD compared to UASb myoblasts. *Dashed horizontal line* denotes a significance threshold of $p < 0.05$. *B*, gene ontology (GO) analysis of cellular component and biological process for proteins exhibiting a lesser turnover rate in FSHD compared to UASb (log_2 Diff. < −1). GO terms were ranked by $-log_{10}$ (q value) and the number of proteins included in each GO term reported alongside each entry. Each bar chart colour scale represents the level of GO enrichment. *C*, density plot of log_{10} transformed fractional protein turnover rate (FTR, %/h) in FSHD and UASb myoblasts. The *vertical black line* in each density plot indicates the median for each sample, whereas the *red vertical line* indicates (0 log_{10}) represents an FTR of 1%/h. No difference in FTR profile (one-way ANOVA, $p = 0.37$) were detected between FSHD and UASb myoblasts. STRING protein interaction networks for proteins with (*D*) lesser turnover rate (log_2 Diff. < −1) or (*E*) greater turnover rate (log_2 Diff. > 1) in FSHD compared to UASb myoblasts. The STRING interaction network was generated using a minimum interaction score of 0.7 and the interaction network was clustered using k-means clustering. Proteins without interaction partners were omitted from visualization.

quantitation. Mass isotopomer information was processed in R version 4.0.3 (R core team., 2016). The incorporation of deuterium into newly synthesized protein causes a decrease in the molar fraction of the monoisotopic (m_0) peak.

$$fm_0 = \frac{m_0}{m_0 + m_1 + m_2 + m_3} \quad (1)$$

Equation 1: fm_0 = molar fraction, m_0 = monoisotopic peak, m_1, m_2, m_3 = mass isotopomers 1 to 3.

Over the duration of the experiment, changes in mass isotopomer distribution follow a nonlinear exponential pattern as a result of the rise-to-plateau kinetics of D_2O-labelled amino acids into newly synthesized proteins. The rate constant (k) for the decay of fm_0 was calculated as a first-order exponential spanning from

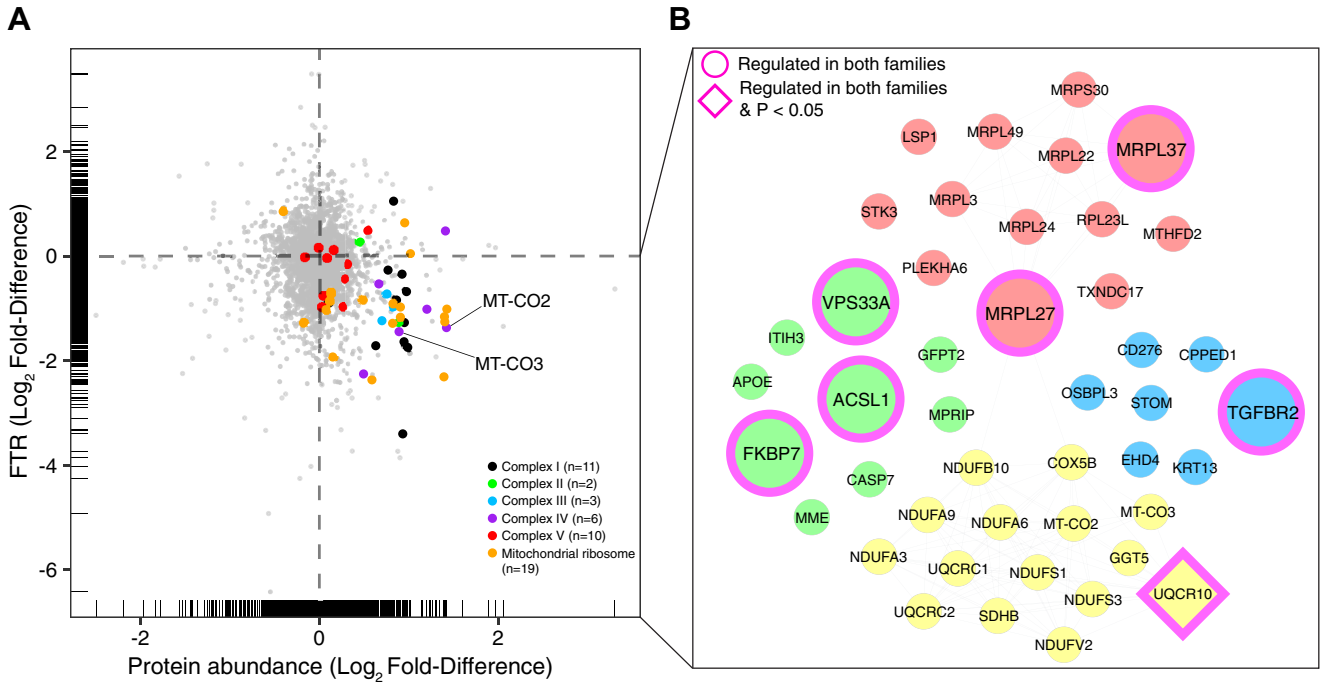

FIG. 4. **Mitochondrial proteins are more abundant but exhibit slower protein turnover rates in FSHD myoblasts.** *A*, scatter plot comparing the differences in the Log_2 Fold-Difference (FSHD/UASb) between protein abundance (x-axis) and protein FTR (y-axis). Rug plots display the distribution of individual data both in X and Y axis. *B*, STRING interaction network of proteins more abundant (log_2 Diff. > 0.6) and slower FTR (log_2 Diff. < −0.6) in FSHD myoblasts. The STRING interaction network was generated using a minimum interaction score of 0.7 and the interaction network was clustered using k-means clustering.

the beginning (t) to the end ($t^{'}$) of the 24 h labeling period, using Equation 2.

$$k = \frac{1}{(t^{'} - t)} \bullet -\ln\left(\frac{fm_{0t}}{fm_{0t^{'}}}\right) \quad (2)$$

Equation 2: k = rate constant, t = first timepoint, $t^{'}$ = end timepoint, fm_{0t} = molar fraction at first timepoint, $fm_{0t^{'}}$ = molar fraction at last timepoint.

Alternatively, the rate constant (k) for the decay of fm_0 for data reported in Figure 6 was calculated as a first-order exponential using fm_0 predicted from the natural isotope pattern of C,H,N,O,S using BRAIN (35) and measurement of fm_0 after 24 h D_2O labeling, using Equation 3.

$$k = \frac{1}{(24)} \bullet -\ln\left(\frac{fm_{0Predict}}{fm_{0Labelled}}\right) \quad (3)$$

Equation 3: k = rate constant, $fm_{0Predict}$ = predicted molar fraction of the monoisotopic peak, $fm_{0t^{'}}$ = measured molar fraction of the monoisotopic peak after 24 h labelling in D_2O.

The rate of change in mass isotopomer distribution is also a function of the number of exchangeable H sites, and this was accounted for by referencing each peptide sequence against standard tables (36) that report the relative enrichment of amino acids by deuterium in humans. Peptide FTR was derived by dividing k by the molar percentage enrichment of ^2H added to the culture media (p) and the total number (n) of ^2H exchangeable H-C bonds in each peptide.

$$FTR = \frac{k}{(n \cdot p)} \quad (4)$$

Equation 4: k = rate constant, n = number of H-D exchange sites, p = precursor enrichment.

The median FTR of peptides assigned to each protein was used to calculate the FTR for each protein in each individual FSHD and UASb sample. Decimal values were multiplied by 100 to give FTR in %/h.

Experimental Design and Statistical Rationale

The experiment was designed to investigate differences in the abundance and turnover rate of proteins that are common between two matched pairs of FSHD and UASb control samples. All statistical analyses were performed using R version 4.2.1. Two-way mixed ANOVA was performed to assess protein abundances in FSHD (n = 2) and UASb (n = 2) samples at baseline (0 h) and 24 h time points and confirm that the abundance of most proteins was stable during the D_2O labeling period. Subsequently, protein abundances measured at baseline and after 24 h of labeling with D_2O were averaged for each biological replicate FSHD (n = 2) and UASb (n = 2), and one-way ANOVA was used to assess differences in protein abundance between FHSD and UASb groups.

Peptide mass isotopomer distributions measured at baseline and after 24 h of labeling with D_2O were used to calculate protein turnover rates in each biological replicate FSHD (n = 2) and UASb (n = 2), and one-way ANOVA was used to assess differences in protein turnover rates between FHSD and UASb groups.

Differences in the abundance or turnover rate of proteins between FSHD and UASb groups are reported as log_2 transformed data and statistical significance was set at $p < 0.05$. Due to the limited number of replicates (n = 2, per group) a false discovery rate criterion was not set, instead, q values (37) at the $p = 0.05$ threshold were reported.

A verification experiment (reported in Fig. 6) was performed using cultures of FSHD and UASb myoblasts that were independent of the

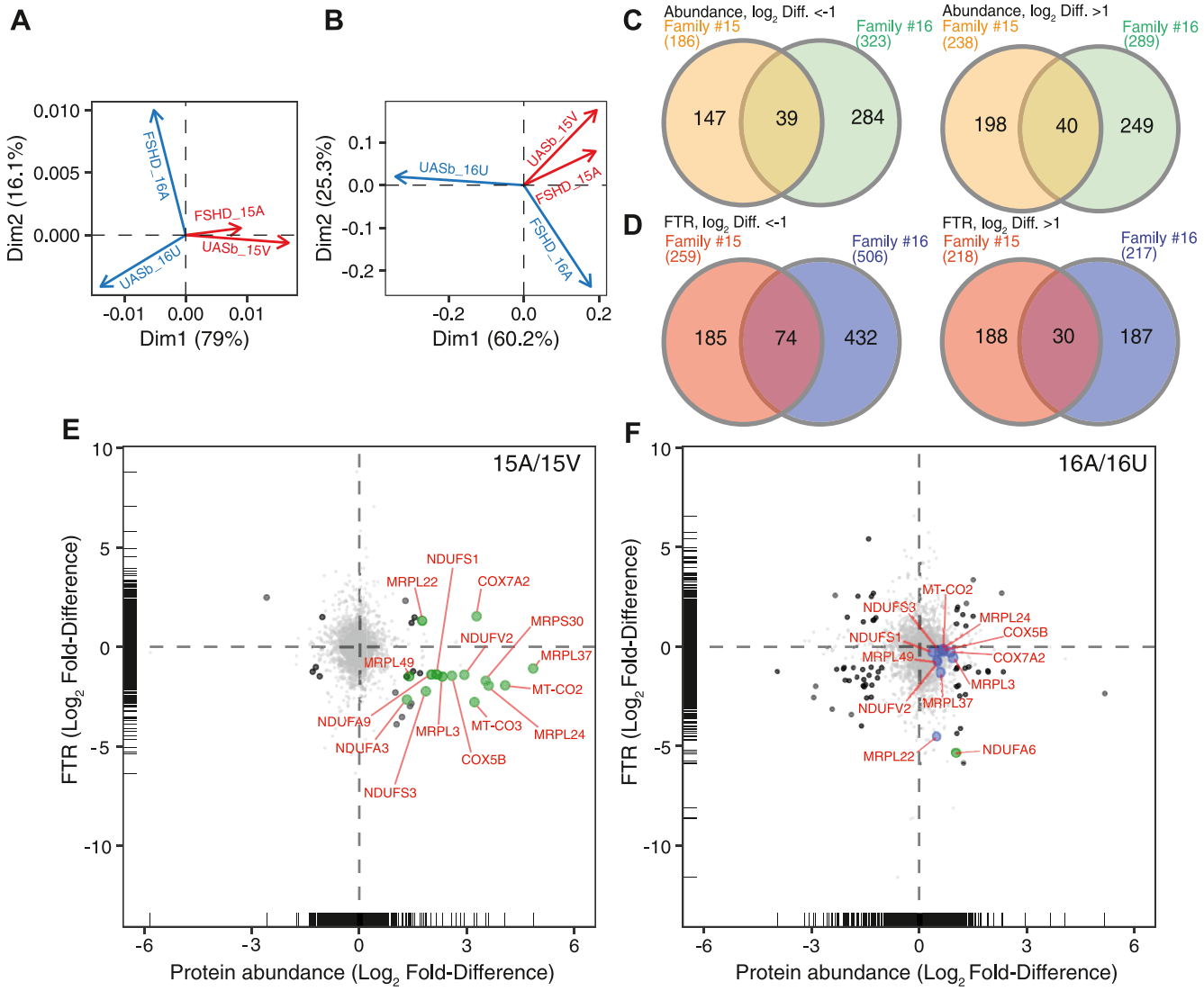

FIG. 5. **Dysregulation of mitochondrial protein is common in FSHD despite variation between families.** Principal Component Analysis (PCA) on (*A*) protein abundance and (*B*) FTR data in FSHD and UASb myoblasts of Family #15 and family #16. Venn diagrams of abundance (*C*) and FTR (*D*) data illustrating the number of strongly regulated (log_2 Diff. > 1 or < −1) proteins common to family #15 and family #16. Scatter plots illustrating family-specific Log_2 Fold-Differences (FSHD/UASb) in protein abundance (x-axis) and protein FTR (y-axis). Black circles represent proteins strongly regulated (log_2 Diff. > 1 or < −1) in abundance and FTR, only mitochondrial proteins were annotated (*green circles*). *Blue circles* in (*F*; family #16A/16U) highlight nine mitochondrial proteins that were strongly regulated in family #15 (*E*).

initial analyses (reported in Figs. 1–5) and cells were cultured with D_2O for 24 h with either 2′-MOE antisense oligomer or vehicle. Protein abundances were measured at the 24 h timepoint only, and the turnover rate of each protein was calculated against predicted baseline values. Differences in protein abundance or protein turnover rates between condition (FSHD *versus* UASb) and treatment (2′-MOE *versus* vehicle) were investigated by independent one-way ANOVAs.

Bioinformatic Analysis

Gene ontology analysis of proteins more enriched (log_2 Diff. > 1) or depleted (log_2 Diff. < −1) in FSHD was performed *via* Over-representation Enrichment Analysis (38) using the Gene Ontology enRIchment anaLysis and visuaLizAtion tool (Gorilla) (39, 40). Enrichment of GO terms was considered significant if the Benjamini and Hochberg adjusted *p* value (41) was <0.01. Protein interactions were investigated using bibliometric mining in the Search Tool for the Retrieval of INteracting Genes/proteins (STRING, Version 11.5) (42), and the interaction networks were illustrated using Cytoscape (Version 3.9.1) (43). InteractiVenn was used to generate Venn diagrams (44). The coverage of mitochondrial Complex subunit proteins and mitochondrial ribosomal proteins was surveyed as identified in Human MitoCarta 3.0 (45).

RESULTS

Protein Abundance Profiling of FSHD and UASb Myoblasts

Label-free quantitation encompassed 4420 proteins in myoblast cultures from two individuals affected by FSHD and

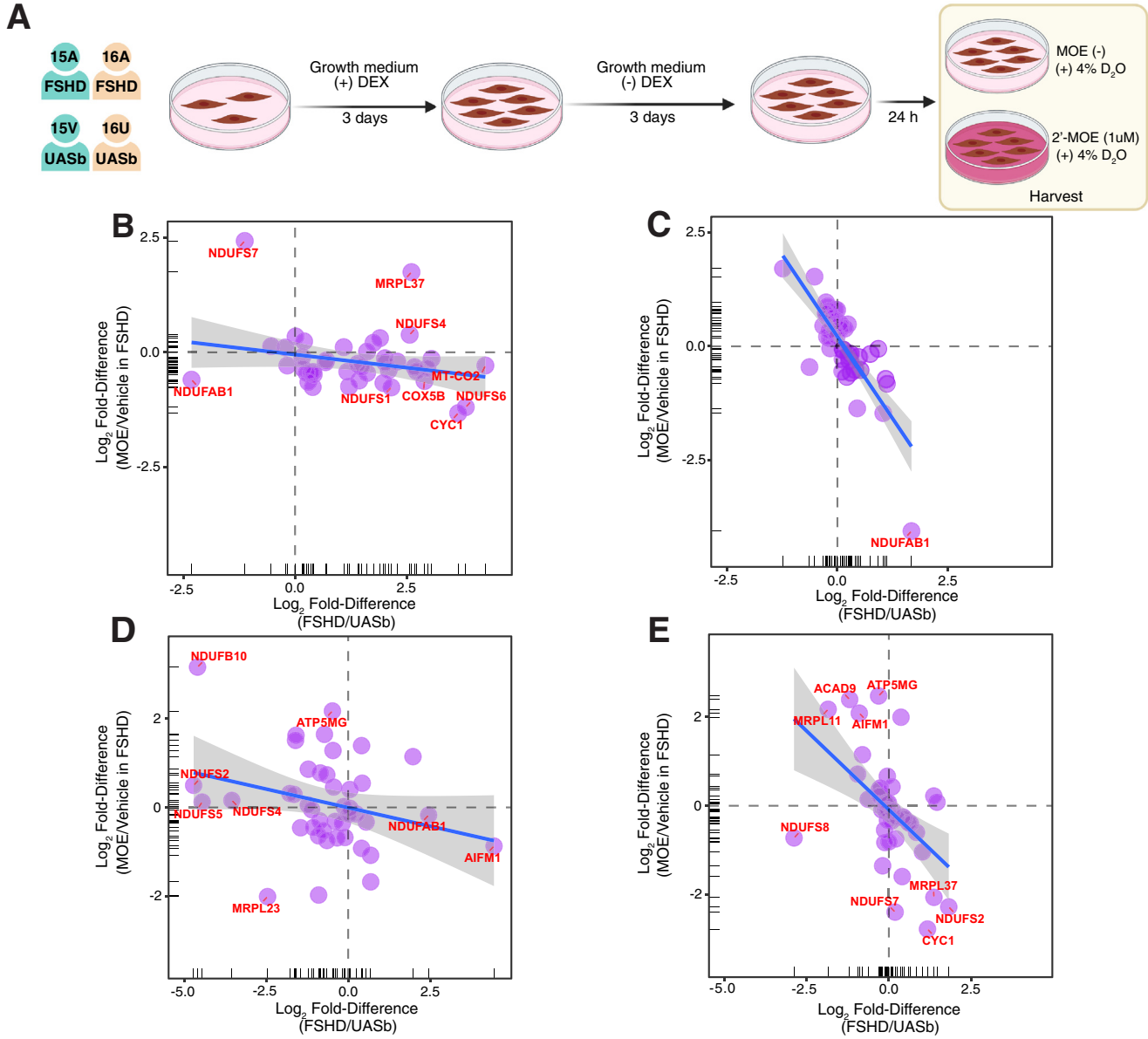

FIG. 6. **Dysregulation of mitochondrial proteins tends to be reversed by 2′-MOE antisense oligomer treatment targeting DUX4.** *A*, experimental design of a subsequent independent study including treatment of FSHD and UASb myoblasts with a 2′-MOE modified antisense oligomer targeting exon three of DUX4. Scatter plots (*B–E*) compare the Log_2 Fold-Difference between FSHD and UASb (x-axis) and the Log_2 Fold-Difference in 2′-MOE treated FSHD myoblasts against vehicle control for abundance data of family #15 (*B*) or family #16 (*C*) and FTR data of family #15 (*D*) or family #16 (*E*). Rug plots display the distribution of data on x-axis and y-axis. A linear regression line with 95% confidence intervals was drawn in each figure panel. The negative slope of the regression line indicates a counter effect of 2′-MOE modified antisense oligomer treatment against FSHD.

their unaffected siblings (UASb), each sampled at two timepoints (baseline and after 24 h labelling with D_2O; Fig. 1*A*). Protein abundances were closely correlated (Pearson's r ≥ 0.958) between sample pairs collected at baseline and 24 h timepoints, and correlations across FSHD and UASb samples, either within or between families, ranged between $r = .93$ and $r = .995$ (Fig. 1*C*). Two-way mixed analysis of variance between groups (FSHD *versus* UASb) and repeated over time (Baseline *versus* 24 h) found no statistical interactions (p values < 0.05) that had a false discovery rate <69%, and just five proteins (EEF2K, MRPL3, BRD3, HSPB3 and PODXL) with an interaction effect ($p < 0.05$, $q > 0.69$) exhibited a >2-fold difference (log_2 Diff. –1 < or 1 >) in protein abundance. 11 proteins (COX7A2L, PTX3, GINM1, MRPL48, UBR3, EFNB1, EEF2K, MRPL3, BRD3, PODXL, and GJA1) exhibited a statistical main-effect of time (p values < 0.05, $q > 0.48$) and a >2-fold difference in protein abundance. Consequently, protein abundance was considered to be stable for the

majority (99.6%) of proteins during the 24 h D_2O-labeling period, and in the analyses below the average of protein abundance values at baseline and 24 h timepoints were used.

One-way analysis of variance of time-averaged abundance data highlighted 114 proteins that exhibited a significant difference ($p < 0.05$) between FSHD *versus* UASb groups, and 17 of these proteins exhibited a greater than 2-fold difference in average protein abundance. Nine proteins (FKBP7, UFSP2, FHL1, EEF2K, USP11, PIP4K2C, NDUFA4, MRPL19, and UQCR11) were more abundant (log_2 Diff. > 1) in FSHD samples and eight proteins (HAUS6, TBC1D22A, MAP3K7CL, FNBP4, CEP170B, CNOT9, TACC3, and CCNA2) were less (log_2 Diff. < −1) abundant in FSHD compared to UASb myoblasts (Fig. 2*A*). In addition, six proteins (DUSP23, ANAPC4, DDX56, PARP12, ZYG11B, and MT-ND4) were detected exclusively in FSHD and three proteins (NPR3, CFB, and FOXO1) exhibited extremely large (64-fold difference; log_2 Diff. > 6) abundance in FSHD compared to UASb. 12 proteins (PHLDA1, ANKRD10, XAF1, DCAF1, DCLRE1C, IGFBP3, PRORP, GNL2, SLC25A23, SECTM1, TOP3B, and FBP1) were uniquely detected in UASb samples and three proteins (ARNTL2, TRIL, and MCM9) exhibited extremely low (−64-fold difference; log_2 Diff. < −6) abundance in FSHD compared to UASb samples. Proteins that exhibited extremely large abundance differences between FSHD and UASb were due to family-specific differences between FSHD and UASb samples (supplemental Fig. S1).

Gene ontology terms that were significantly enriched amongst proteins depleted (log_2 Diff. < −1) in FSHD myoblasts, included extracellular matrix and biological processes associated with intermediate filament organization (Fig. 2*B*). Protein interaction networks of those less abundant in FSHD samples formed four dominant clusters (Fig. 2*D*), encompassing (i) DNA replication and mitotic cell cycle processes (green), (ii) cytoskeleton organization (yellow), (iii) mediator of RNA polymerase II transcription (blue), and (iv) mTOR signaling proteins (red).

Biological processes associated with mitochondrial translation and the respiratory electron transport chain were significantly enriched amongst proteins that were more abundant (log_2 Diff. > 1) in FSHD myoblasts (Fig. 2*C*). Our analysis encompassed 75%, 50%, 80%, 48% and 62% of protein subunits of respiratory chain complexes I-V, respectively. With the exception of UQCRQ (log_2 Diff. −0.56) of Complex III and Complex V subunits ATP5PD (log_2 Diff. −0.16), ATP5ME (log_2 Diff. −0.59), and ATP5F1B (log_2 Diff. −0.014), all other respiratory chain proteins were more abundant (log_2 Diff. ranging from 0.1 to 2.6) in FSHD samples. Specifically, three subunits of the respiratory chain complex IV were 2-fold more abundant in FSHD myoblasts, including COX5B, COX7A2, and MT-CO2 although statistical significance was not evident ($p > 0.05$). Sixty-one out of 83 known mitochondrial ribosomal proteins were included in our analysis (73% coverage) and all mitochondrial ribosomal proteins apart from (DAP3, MRPS17, MRPS18B, MRPS25, MRPS28, MRPS35) were more abundant (log_2 Diff. ranging from 0.016 to 2.5) in FSHD myoblasts when compared to UASb. Specifically, five mitochondrial ribosomal proteins were 2-fold more abundant in FSHD myoblasts, including MRPL39, MRPL27, MRPL37, MRPL24, and MRPL3 although statistical significance was not evident ($p > 0.05$). Furthermore, the protein interaction networks derived from proteins that were more abundant in FSHD samples formed four dominant clusters (Fig. 2*E*), encompassing (i) mitochondrial ribosomal proteins (yellow), (ii) mitochondrial respiratory chain components (green), (iii) FOXO-mediated transcription (red), and (iv) positive regulation of cyclin-dependent protein kinase activity (blue).

Differences in Protein Fractional Turnover Rate (FTR) Between FSHD and UASb Myoblasts

Turnover rates were calculated for 2324 proteins that had high-quality peptide mass isotopomer data available at baseline and after 24 h of D_2O labeling in n = 2 FSHD and n = 2 UASb samples (Fig. 3*A*). Deuterium incorporation data were unavailable for the five proteins that exhibited a significant interaction between group and time or the 11 proteins that exhibited a significant main effect of time therefore the contributions of synthesis and degradation to the changes in protein abundance could not be investigated, unlike our previous study (33). The median turnover rate amongst proteins in FSHD myoblasts (15A: 0.58%/h, 16A: 0.43%/h) was not significantly ($p = 0.37$) different from that exhibited by UASb myoblasts (15 V: 0.60%/h, 16U: 0.51%/h), but the distribution of protein-specific turnover rates in UASb samples was shifted rightward (faster rates of protein turnover) compared to FSHD samples (Fig. 3*C*). One-way analysis of variance (FSHD *versus* UASb) highlighted 77 proteins that exhibited statistically significant ($p < 0.05$) differences in turnover rate between FSHD and UASb myoblasts (Fig. 3*A*). Thirty-seven of the statistically significant proteins exhibited a >2-fold difference (log_2 Diff. > 1) in turnover, including 11 proteins that had faster rates of turnover in FSHD samples and 26 proteins that had slower rates of turnover compared to UASb samples.

The gene ontology terms, including mitochondrial protein complex and mitochondrial large ribosomal subunit and biological processes associated with mitochondrial translational termination and elongation were significantly enriched amongst proteins that exhibited slower (log_2 Diff. < −1) rates of turnover in FSHD myoblasts. Protein that had slower rates of turnover in the FSHD samples formed five clusters (Fig. 3*D*), encompassing (i) mitochondrial respiratory chain complex I assembly (purple), (ii) regulation of mRNA processing and proteasome (yellow), (iii) mitochondrial outer membrane translocase complex (green), (iv) ribosomal large subunit assembly and biogenesis (red), and (v) cellular metabolic process (light blue).

No significantly enriched gene ontology terms were detected amongst proteins that exhibited greater (log_2 Diff. > 1) turnover in FSHD myoblasts. Protein interaction networks

drawn from proteins that had greater rates of turnover in FSHD compared to UASb samples formed three clusters (Fig. 3*E*), which were manually curated as (i) cellular protein localization (green), (ii) extracellular exosome (red), and (iii) tight junction (blue).

Comparison of Protein Abundance and Turnover Data

Differences in protein abundance and turnover data between FSHD and UASb were plotted alongside one another in a scatterplot. The top-left quadrant includes proteins less abundant but greater in turnover rate in FSHD myoblasts. The top-right quadrant includes proteins more abundant with a greater turnover rate in FSHD myoblasts. The bottom-left quadrant includes proteins that were less abundant and exhibited lesser protein turnover in FSHD myoblasts. The bottom-right quadrant includes proteins that were more abundant but exhibit a slower rate of turnover in FSHD myoblasts. Stringent criteria (STRING high confidence (0.7) interaction score, $\log_2$ Diff. > 0.6) were used to highlight core clusters of proteins that share similar patterns across the two pairs of patient and sibling samples (Fig. 4*A*). In all, 11 subunits of mitochondrial Complex I proteins had both abundance and FTR data, and ten proteins (NDUFA3, NDUFA6, NDUFA8, NDUFA9, NDUFB10, NDUFB11, NDUFS1, NDUFS3, NDUFS6, and NDUFV2) were located in the bottom right quadrant (black dots). Two subunits of mitochondrial Complex II proteins had both abundance and FTR data, and SDHB was found in the bottom right quadrant (green dots). Three subunits of mitochondrial Complex III proteins had both abundance and FTR data, and each of these proteins (UQCR10, UQCRC1, and UQCRC2) was located in the bottom right quadrant (light blue dots). Six subunits of mitochondrial Complex IV proteins had both abundance and FTR data, and five proteins (COX4I1, COX5A, COX5B, MT-CO2, and MT-CO3) were located in the bottom right quadrant (purple dots). Notably, mitochondrially encoded gene products, MT-CO2 and MT-CO3 (subunits of mitochondrial Complex IV) were also located in the bottom right quadrant. Abundance and FTR data were measured for ten subunits of mitochondrial Complex V, and seven proteins (ATP5F1C, ATP5MF, ATP5MG, ATP5PB, ATP5PD, ATP5PF, and ATP5PO) were located in the bottom right quadrant (red dots). In all, 19 mitochondrial ribosomal proteins had both abundance and FTR data, and 16 of these (MRPL1, MRPL12, MRPL22, MRPL23, MRPL24, MRPL27, MRPL3, MRPL37, MRPL49, MRPS14, MRPS28, MRPS30, MRPS31, MRPS36, MRPS5, and PTCD3) were located in the bottom right quadrant (orange dots). In accordance with the GO analysis of protein abundance and protein turnover data, these proteins are more abundant in FSHD but have a slower turnover rate compared to UASb. Interaction networks (Fig. 4*B*) of proteins that were more abundant ($\log_2$ Diff. > 0.6) and had slower rates of turnover ($\log_2$ Diff. < –0.6) in FSHD myoblasts formed two major clusters, encompassing (i) mitochondrial respiratory chain complex I assembly (yellow) and (ii) mitochondrial translational elongation and termination (red).

Family-Specific Analysis Revealed Accumulation of Mitochondrial Proteins as a Common Feature in FSHD Myoblasts

Differences in protein abundance profile (Fig. 5*A*) and FTR (Fig. 5*B*) between families were larger than or equal to the magnitude of difference between FSHD and UASb samples. Nevertheless, family #15 and family #16 exhibited shared differences between FSHD and UASb samples in both protein abundance (Fig. 5*C*) and protein FTR (Fig. 5*D*). Thirty-nine proteins were commonly less abundant in FSHD samples. Six of these proteins (HAUS6, TBC1D22A, MAP3K7CL, FNBP4, CEP170B, and CNOT9) had exhibited significant (p < 0.05) differences in average abundance (Fig. 2, *A* and *D*), whereas 17 proteins and 23 proteins were more strongly regulated in either family #15 or #16, respectively (supplemental Fig. S2). Amongst the 40 proteins that were commonly more abundant in FSHD, five of these proteins (USP11, PIP4K2C, NDUFA4, MRPL19, and UQCR11) had exhibited significant (p < 0.05) differences in average abundance (Fig. 2, *A* and *E*), whereas 18 proteins and 21 proteins were more strongly regulated in either family #15 or #16, respectively (supplemental Fig. S2). Eight mitochondrial proteins (MRPL50, COX6B1, NDUFA4, MRPL19, NDUFB1, MRPL58, MRPL13, and UQCR11) exhibited a relatively larger difference between FSHD and UASb in family #15, but, nevertheless, a greater abundance of these proteins in FSHD was common in both family #15 and family #16.

The FTR of 74 proteins was commonly less in FSHD and UASb and 18 of these proteins had exhibited statistically significant (p < 0.05) differences in average FTR (Fig. 3, *A* and *D*). Five mitochondrial proteins (UQCR10, MRPL1, MRPS31, MRPL37, and NDUFB10) commonly had lesser FTR in FSHD than UASb samples, but the magnitude of difference between FSHD and UASb was greater in family #15 for UQCR10 and MRPL1 or greater in family #16 for proteins MRPS31, MRPL37, and NDUFB10 (supplemental Fig. S2). Among the 30 proteins that exhibited commonly greater FTR in FSHD samples, nine proteins (LAMB1, GNAQ, SCRIB, RAB32, AP3B1, ELOB, ITGB5, P3H1, and LMF2) had exhibited significant (p < 0.05) differences in average FTR (Fig. 3, *A* and *E*), whereas eight proteins and 22 proteins were more strongly regulated in family #15 and #16, respectively (supplemental Fig. S2). The commonality of mitochondrial proteins th\o "appsec1" at differ between FSHD and UASb but distraite magnitude of responses between family #15 and family #16 are illustrated in Figure 5, *E* and *F*.

Antisense Oligonucleotide Treatment Counteracts Mitochondrial Protein Dysregulation in FSHD Myoblasts

Differences in the abundance and FTR of proteins between FSHD and UAsb were independently verified in a separate

experiment (Fig. 6*A*) that included treatment with a 2′-MOE modified antisense oligonucleotide targeting exon three of the DUX4 transcript (30). This experiment, which encompassed abundance data for 3462 proteins and FTR data for 2251 proteins, agreed closely with the findings of the preceding analysis. Mitochondrial proteins were, again, more abundant in FSHD as compared to UASb (supplemental Fig. S3*A*), and one-way analysis of variance highlighted 40 proteins that exhibited significant differences ($p < 0.05$) in abundance (supplemental Fig. S4*A* and supplemental Table. S3). Similarly, the FTR of mitochondrial proteins was slower in FSHD as compared to UASb (supplemental Fig. S4*B* and supplemental Table. S4), and one-way analysis of variance highlighted 77 proteins that exhibited a significant difference ($p < 0.05$) between FSHD and UASb groups. Accordingly, duplicate independent analysis of protein abundance and FTR differences between FSHD and UASb myoblasts highlighted a pattern of heightened abundance but slowed the turnover rate of mitochondrial proteins (supplemental Fig. S4*C*).

Abundance and FTR data were reported for 43 mitochondrial proteins in FSHD and UASb samples from both family #15 and family #16, treated with or without the 2′-MOE antisense oligonucleotide (Fig. 6, *B–E*). Mitochondrial proteins that were more abundant in FSHD than UASb tended to exhibit lower abundance after 2′-MOE antisense oligonucleotide treatment and were located in the bottom right quadrants. Linear regression analyses highlight greater responses to MOE in family #16 than family #15 for both protein abundance (family #15 slope = −0.114 Fig. 6*B*, family #16 slope = −1.44 Fig. 6*C*) and protein FTR (family #15 slope = −0.167 Fig. 6*D*, family #16 slope = −0.706 Fig. 6*E*).

DISCUSSION

We have used proteomic analysis of stable isotope-labeled patient-derived myoblasts to generate new insight into the potential disease mechanisms of FSHD. Our global proteomic data on the abundance and turnover of individual proteins highlighted that mitochondrial proteins, particularly subunits of the mitochondrial respiratory complexes and mitochondrial ribosomal proteins, were more abundant and had slower rates of turnover in FSHD myoblasts. These findings suggest mitochondrial protein quality might be impaired in FSHD, and FSHD myoblasts may exhibit an accumulation of “older” less viable mitochondrial proteins. Indeed, the response (difference in abundance and difference in turnover rate) of mitochondrial proteins to FSHD, was counteracted (Fig. 6) by treating FSHD myoblasts with an antisense oligomer that suppresses the expression of DUX4 (30). Our proteomic dataset also adds new detail to previously known aspects of FSHD muscle pathology, including defects in RNA processing, cell cycle regulation, stress kinase pathways, and apoptosis. Our data from two matched pairs of individuals with FSHD and unaffected siblings provide an impetus for further exploration of the role of post-transcriptional processes in the pathophysiological mechanisms of FSHD.

Recently, Heher *et al.* (8) reported the severity of FSHD is positively associated with a lower expression of mitochondrial genes in both skeletal muscle biopsies and myoblasts from individuals affected with FSHD. One of the pairs of FSHD and UASb myoblast samples (16A and 16U) analyzed in the current work were also included in the report by Heher *et al.* (8). Taken together, the differences in gene expression (decreased in FSHD; (8)), protein abundance (increased in FSHD), and protein turnover (decreased in FSHD) of mitochondrial proteins (Fig. 4) suggest FSHD myoblasts are characterized by an accumulation of older, potentially less viable, mitochondrial proteins. Most mitochondrial proteins are transcribed from nuclear genes then synthesized in the cytosol and transported into mitochondria, whereas 13 proteins originate from mitochondrial DNA (mtDNA) and contribute subunits to the respiratory chain complexes (45). Our proteomic analysis encompassed approximately half (6 out of 13 proteins) of mtDNA-encoded proteins, and each of the mtDNA-encoded proteins was more abundant in FSHD myoblasts (supplemental Table S1). Protein turnover data was available for two mitochondrially encoded proteins MT-CO2 (a subunit of Complex IV) and MT-ATP6 (a subunit of Complex V) and each of these proteins were included among the cluster of nuclear-encoded proteins that were more abundant (>2-fold difference; $\log_2$ Diff. > 1) but had slower rates of turnover in FSHD myoblasts (Fig. 4, *A* and *B*). Our analysis does not specifically distinguish between mitochondrial proteins that were resident within or outside mitochondria during the study period. Nevertheless, the similarities between nuclear-encoded and mitochondrially encoded proteins may indicate a disease mechanism involving the degradation of proteins within mitochondria rather than an interruption to the transport and degradation of proteins destined for mitochondrial import.

Quadriceps muscle of individuals affected by FSHD exhibits mitochondrial dysfunction and evidence of oxidative stress, including lipofuscin inclusions and protein carbonylation, which correlate with the severity of muscle functional impairments (46). Furthermore, transmission electron microscopy (46) revealed areas of accumulated mitochondrial proteins were associated with myofibrillar disorganization, badly formed mitochondrial cristae, swelling, or separation of the inner and outer membranes in FSHD-affected muscles. Laoudj-Chenivesse *et al.* (16) reported that proteins involved in mitochondrial oxidative metabolism, such as complex I subunits, NADH dehydrogenase flavoprotein (NDUFV), and NADH-ubiquinone oxidoreductase (NDUFA) are more abundant in both clinically affected and unaffected individuals with FSHD when compared to control subjects. However, mitochondrial disturbances and indicators of oxidative stress were less apparent in clinically affected biceps or deltoid muscle compared to muscles, such as quadriceps, that do not exhibit overt clinical signs of FSHD pathology (16). Previously, the

FSHD patient-derived immortalized cells used in this study could not be distinguished from healthy controls based on their response to cellular stresses, including hydrogen peroxide and glutathione depletion (21), unlike other studies that used immortalized cells (5, 19). FSHD myoblasts can repair DNA damage caused by moderate levels of oxidative stress but fail to recover from higher levels or chronic exposure to oxidative stress (47). Using myoblasts from individuals with FSHD and normal control, Winokur *et al.* (5) demonstrated that FSHD myoblasts are more susceptible to oxidative stress and had lower levels of expression of genes involved in antioxidant processes, such as Glutathione S-transferase theta-2 (GSTT2), Glutathione reductase (GSR), and Heat shock 70 kDa protein 4 (HSPA4). Our proteomic analysis also found that GSTT2 and HSPA4 were less abundant in FSHD myoblasts while GSR was more abundant in FSHD myoblasts (supplemental Table S1), suggesting a heightened oxidative stress and a potential connection to mitochondrial dysfunction.

Apoptosis is one of the affected biological pathways in individuals with FSHD (48, 49) and mitochondria have been shown to contribute to the regulation of apoptosis *via* mitochondrial-derived cytochrome *c* (50). Previous studies suggested that apoptosis can be induced *via* an increase in mitochondrial ribosome proteins, such as MRPS30 (51) and MRP41 (52). Our proteomic analysis detected a higher abundance of each of these mitochondrial ribosomal proteins in FSHD myoblasts (Fig. 4*B* and supplemental Table S1). MRPS30 and MRP41 proteins were reported to induce apoptosis *via* different mechanisms, for example, MRP41 has been reported to induce apoptosis *via* both p53-dependent (53) and p53-independent (54) pathways. Conversely, Sun *et al.* (51) demonstrated that overexpression of MRPS30 induces apoptosis while increasing transcription factor c-Jun and activating of c-Jun N-terminal kinase 1 (JNK1) in mouse fibroblasts. Consistently, our proteomic analysis detected that transcription factor AP-1 (JUN) is enriched in FSHD myoblasts (Fig. 2*E*). Dual specificity protein phosphatase 23 (DUSP23) was also enriched in FSHD myoblasts (Supplemental Fig. S1 and Supplemental Table S1) and is known to enhance the activation of JNK, which is a recognized downstream target of DUX4 (55). In support of activation of apoptosis, several caspase proteins were more enriched in FSHD myoblasts, including caspase-9 (CASP9) and caspase-7 (CASP7) (Fig. 4*B* and Supplemental Table S1), although the activation status of these proteins cannot be ascertained without knowing their cleavage status. Nevertheless, our data are consistent with recent data (15) linking DUX4 induction with increases in the proportion of Caspase 3/7 positive cells. Several proteins that were uniquely detected in FSHD sample 16A, indicate heightened caspase activity, including protein zyg-11 homolog B (ZYG11 B), which is a substrate adaptor subunit in the E3 ubiquitin ligase complex ZYG11B-CUL2-Elongin BC, and plays a role in the clearance of proteolytic fragments generated by caspase cleavage during apoptosis (56). In addition, FOXO1, a transcription factor targeting apoptosis signaling, was particularly more abundant in FSHD sample 16A (FSHD) as compared to 15A (FSHD) (supplemental Fig. S1). These findings suggest sample 16A may exhibit higher caspase activity and a more severe FSHD phenotype than sample 15A.

Antioxidant agents may rescue the impairments in muscle function exhibited by individuals affected with FSHD (57, 58). Antioxidants ameliorate several FSHD-related dysregulated biological pathways, including oxidative DNA damage (6) and apoptosis (59) *via* a possible suppression of DUX4 transcription. In particular, mitochondrial-targeted antioxidants are more potent than non-targeted agents (8), which suggests respiratory chain dysfunction may be a major contributor to the pathological generation of reactive oxygen species (ROS). Our discovery that subunits of the respiratory chain complexes exhibit a slower rate of turnover in FSHD-affected myoblast may point to losses in mitochondrial protein quality control or possibly mitophagy as an underlying mechanism in FSHD. Indeed, Lei *et al.* (60) report impairments in mitophagy result in an accumulation of dysfunctional mitochondrial excessive mitochondrial ROS generation.

Overexpression of DUX4 in MB135 myoblasts is associated with a 50% decrease in protein synthesis (13). We also report the median turnover rate of proteins is lesser in FSHD compared to UASb myoblasts (Fig. 3*C*). Our proteomic data reveal protein-specific differences in turnover rate between FSHD and UASb samples (Fig. 3*C*) and discordance between protein turnover and protein abundance data (Fig. 4*A*). The median turnover rate of proteins was less in FSHD sample 16A compared to FSHD sample 15A, and protein mono-ADP-ribosyltransferase PARP12 (PARP12) was specifically detected in 16A (FSHD) (supplemental Fig. S1). PARP12, a member of a large family of ADP-ribosyl transferases, can be recruited to stress-granules (*i.e.*, known sites of mRNA translation arrest) and block mRNA translation (61), which may contribute to the greater impairment of protein synthesis FSHD sample 16A. In agreement with Jagannathan *et al.* (13), we found proteins involved in the negative regulation of protein synthesis were more abundant in FSHD myoblasts, including eukaryotic elongation factor 2 kinase (EEF2K) (Fig. 2*A*), which inhibits translation elongation. Jagannathan *et al.* (13) report the phosphorylation of eIF2a is increased in a time-dependent manner after DUX4 induction (*i.e.*, indication of translation inhibition) with a concomitant decrease in [^{35}S]-Methionine incorporation. In our data, other proteins associated with the positive regulation of protein synthesis were less abundant in FSHD myoblasts, including large neutral amino acids transporter small subunit 1 (SLC7A5), RAC-gamma serine/threonine-protein kinase (AKT3), Hamartin (TSC1), and Rapamycin-insensitive companion of mTOR (RICTOR) (Fig. 2*D* and supplemental Table S1). However, the kinase activity of these

proteins involved in the mTOR signaling pathway remains to be investigated.

FSHD is associated with a progressive decline in muscle mass and our proteomic analysis detected proteins associated with negative regulation of skeletal muscle growth, including Growth/differentiation factor 8 (MSTN) and Tensin-2 (TNS2), which were more abundant in FSHD myoblasts (Fig. 2*E* and supplemental Table S1). Moreover, the GO biological process-terms depleted in FSHD myoblasts included positive regulation of cell proliferation (Fig. 2*B*), based on the finding that Cyclin-dependent kinase 6 (CDK6), Cyclin-A2 (CCNA2), Cyclin-dependent kinase 13 (CDK13), Cyclin-dependent kinase 9 (CDK9) were decreased (Fig. 2*D* and supplemental Table S1). Conversely, proteins associated with a negative regulation of cell cycle, such as Cyclin-dependent kinase inhibitor 1B (CDKN1B), Cyclin-dependent kinase inhibitor 1 (CDKN1A), Cyclin-dependent kinase four inhibitors (CDKN2C), Cyclin-dependent kinase inhibitor 1C (CDKN1C), Cyclin-dependent kinase four inhibitor B (CDKN2B) were increased (Fig. 2*E* and supplemental Table S1). Cyclin-dependent kinase (Cdk) is activated by association with cyclin subunits and phosphorylation of the Cdk subunit by the Cdk-activating kinase. Thus, Cdk activity and the profile of cell cycle phases warrant further investigation in FSHD and UASb myoblasts.

Human myogenic cells expressing DUX4-FL exhibit insoluble ubiquitylated proteins (48), which suggests the ubiquitin-proteasome system may be impaired in FSHD. Furthermore, proteins involved in the ubiquitin-proteasome system are increased at the transcriptional and protein level (13, 62, 63) after induction of DUX4. In our data, several ubiquitin E2 conjugating enzymes (UBE2T, UBE2D2, UBE2Q1), ubiquitin E3 ligases (UBR3, UBR7, XIAP, TRIM32, RNF149, RNF213), deubiquitylating enzymes (USP11, USP8, USP22, OTULIN, UCHL1), as well as proteasome activator complex subunit protein (PSME4) were each more abundant in FSHD myoblasts (Fig. 2, *A* and *E* and supplemental Table S1) but, nevertheless, protein turnover rates were generally lower. The forkhead box protein O1 (FOXO1) and forkhead box protein O3 (FOXO3) transcription factors (64), which are master regulators ubiquitin E3 ligase proteins (65, 66) and the autophagy lysosome (67, 68), were also more abundant in FSHD myoblasts (Fig. 2*E* and supplemental Table S1). Proteins involved in the autophagy-lysosome system (TM9SF1) and protein quality control (HSPA1L, HSPA14, SGTA) are also more abundant in FSHD myoblasts (supplemental Table S1). Conversely, several small heat shock proteins (HSP) were less abundant in FSHD compared to UASb myoblasts (Fig. 2*D*), including HSPB2, HSPB6, and HSPB3 (Fig. 2*D* and supplemental Table. S1). The FTR of HSPB2 and HSPB6 were also lesser in FSHD than UASb myoblasts (supplemental Table. S2). The differences in abundance and turnover rate of small HSP, which guard against stress-induced protein unfolding and aggregation (69, 70), may indicate the impaired cellular protein quality control that leads to the accumulation of damaged proteins in FSHD muscles.

We measured the abundance of 4420 proteins and the turnover rate of 2324 proteins in each (n = 4) myoblast sample. This proteome coverage compares well against recent abundance profiling of 4005 proteins in MB135 myoblasts (13) and earlier proteome dynamic studies, including Cambridge *et al.* (71) which reported turnover rates for 3528 proteins using dynamic SILAC (stable isotope labeling by amino acids in cell culture) in the murine C2C12 muscle cell line. However, the median half-life of proteins in patient-derived myoblast cultures ($t_{1/2}$ ~ 130 h; Fig. 3) was approximately three-fold greater than the median value ($t_{1/2}$ ~ 43 h) reported in the C2C12 cell line using dynamic SILAC (71) or D2O labeling (34). Despite relatively deep coverage of the myoblast proteome, we did not detect previously suggested FSHD or DUX4 candidate genes highlighted in the biomarker list reported in Yao *et al.* (72). This is unsurprising because DUX4 is transiently expressed and challenging to detect in FSHD patient samples. Moreover, we studied FSHD myoblasts in growth media, conditions that are not expected to be associated with high levels of DUX4 expression (29). Nevertheless, our proteomic data align well with the wider literature on the molecular mechanisms of FSHD. Notably, when DUX4 is artificially expressed in human myoblasts, only eight of 25 candidate genes (72) were detected at the protein level (13). Moreover, almost half (6 of 13) of the FSHD patient samples reported by Yao *et al.* (72) did not show enrichment of the list of DUX4 target genes. The mitochondrial ADP:ATP carrier, ANT1 (also known as SLC25A4), resides in the 4q35 region alongside DUX4 (16) and has also been a focus of interest in FSHD research. We did detect ANT1 but did not find significant differences in either the abundance or turnover rate of ANT1 between FSHD and UASb myoblasts. Our ANT1 data agree with Klooster *et al.* (73) but contrast with Gabellini *et al.* (74) which demonstrated that ANT1 was more abundant in the muscle of both in clinically affected and unaffected individuals with FSHD compared to healthy control subjects.

The clinical heterogeneity of FSHD is well established and, in agreement with the original characterization of these cells (21), interfamily differences were evident in our proteomic analyses of patient-derived myoblast cultures. Between-family differences were of greater magnitude than the differences between FSHD and UASb (Fig. 5, *A* and *B*) but, nevertheless, dysregulation of mitochondrial proteins was evident in FSHD myoblasts of both family #15 and family #16 (Fig. 5, *C* and *D*), albeit to different extents. Family #15 comprises a male individual with FSHD compared against their female UASb, whereas myoblasts of family #16 were generated from sisters with and without FSHD. Inducible expression of DUX4-fl in the muscle of adult mice tends to have greater detrimental effects on muscle function in females than males (75), therefore, we cannot rule out sexual dimorphism as a contributing factor to the observed inter-family differences. Nevertheless, evidence

of dysregulation of mitochondrial proteins in FSHD myoblasts was reproducible and tended to be reversed in myoblasts treated with an antisense oligomer (Fig. 6) previously shown to silence DUX4 mRNA expression (30).

CONCLUSION

Dynamic proteome profiling has offered new insight into the disease mechanisms of FSHD that are underpinned by post-transcriptional processes and effects on protein turnover. We discovered that FSHD myoblasts exhibit a greater abundance but slower turnover rate of mitochondrial respiratory complex subunits and mitochondrial ribosomal proteins, which may indicate an accumulation of "older" less viable mitochondrial proteins (Fig. 7). Antisense oligomer treatment tended to reverse mitochondrial protein dysregulation in FSHD myoblasts, highlighting the role of DUX4-dependent mechanisms in the disruption of mitochondrial proteome dynamics. Our data provide a new hypothesis-generating resource for future mechanistic studies in FSHD, including studies on mitochondrial function and muscle aerobic capacity in FSHD pathology.

DATA AVAILABILITY

The mass spectrometry proteomics data generated in this study have been deposited to the ProteomeXchange Consortium *via* the PRIDE (76) under the dataset identifiers PXD038818 and 10.6019/PXD038818 and PXD042374 and 10.6019/PXD042374.

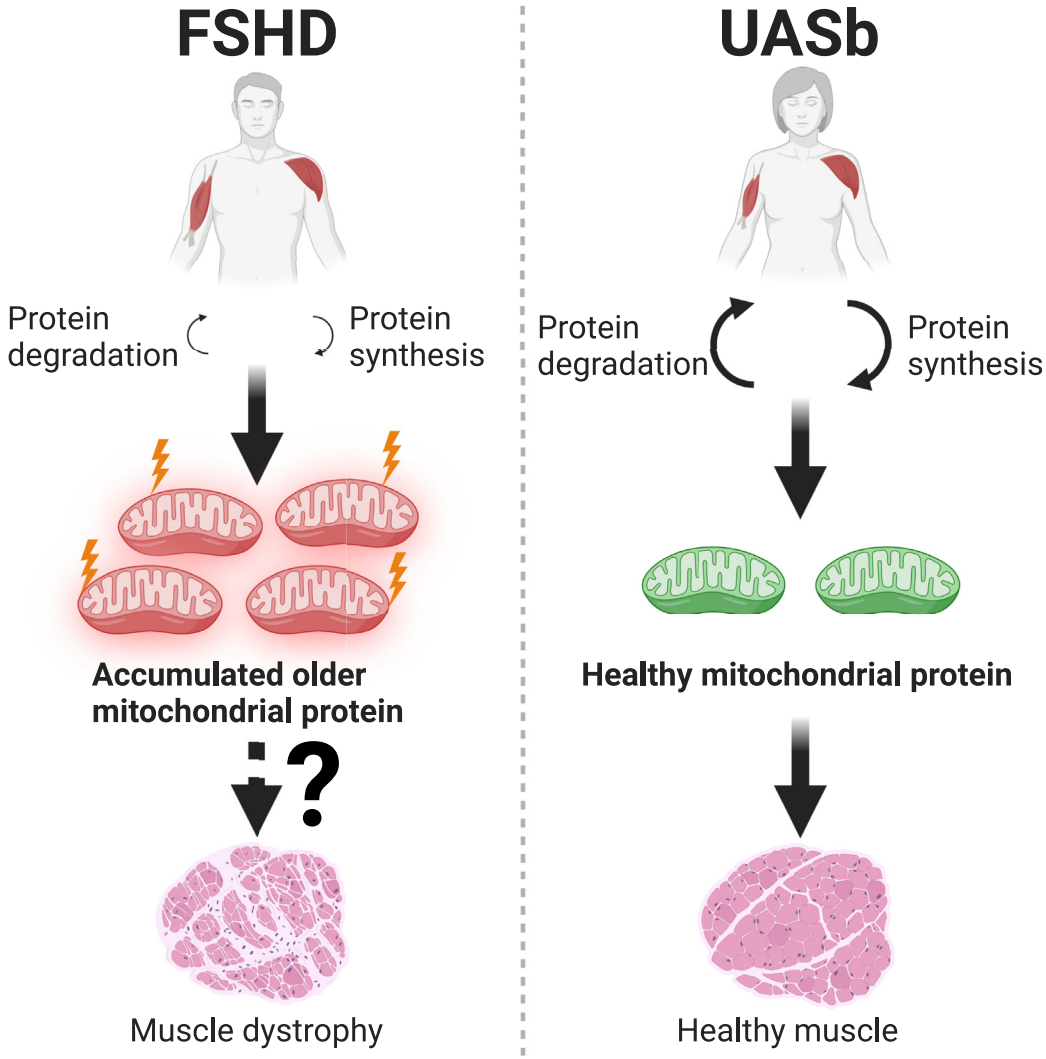

FIG. 7. **Accumulation of "older" less viable mitochondrial proteins may contribute to the pathophysiology of FSHD.** FSHD myoblasts exhibit a greater protein abundance but a slower turnover rate of mitochondrial respiratory complex subunits and mitochondrial ribosomal subunits, which may indicate an accumulation of 'older' less viable mitochondrial proteins compared to UASb myoblasts. This may contribute to the reduced respiratory function specifically observed in Complex I as recently shown by Heher *et al.* (8) in DUX4 expressing iDUX4 myoblasts. Impaired mitochondrial function is proposed as one of the major pathophysiological mechanisms of FSHD. Created with BioRender.com.

Supplemental Data—This article contains supplemental data.

Funding and additional information—Muscular Dystrophy Association – Strength, Science, and Stories of Inspiration Fellowship (A. J. B.), Muscular Dystrophy UK (Y. N., Y.-W. C. and J. G. B.), FSHD Canada (Y.-W. C.), FSHD Society Grant Award (A. J. B.), and American Physical Therapy Association New Investigator Fellowship Training Initiative (A. J. B.).

Author contributions—Y.-W. C. and J. G. B. conceptualization; J. G. B. data curation; Y. N., A. J. B., C. A. S., and J. G. B. formal analysis; Y.-W. C. funding acquisition; Y. N., A. J. B., and C. A. S. investigation; A. J. B., Y.-W. C., and J. G. B. methodology; Y.-W. C. project administration; Y.-W. C. and J. G. B. resources; J. G. B. supervision; Y.-W. C. and J. G. B. supervision; Y. N. and C. A. S. visualization; Y. N. and J. G. B. writing–original draft; Y. N., A. J. B., C. A. S., Y.-W. C., and J. G. B. writing–review and editing.

Conflict of interest—The authors declare that they have no known competing financial interests or personal relationships that could have appeared to influence the work reported in this paper.

Abbreviations—The abbreviations used are: 2′-MOE, 2′-O-methoxyethyl; Ambic, ammonium hydrogen bicarbonate; BSA, bovine serum albumin; D2O, deuterium oxide; DTT, dithiothreitol; DUX4, double homeobox 4; DUX4-FL, full-length isoform of DUX4; FASP, Filter-Aided Sample Preparation; FSHD, facioscapulohumeral muscular dystrophy; FTR, fractional turnover rate; GO, gene ontology; HSP, heat shock proteins; mtDNA, mitochondrial DNA; PCA, principal component analysis; ROS, reactive oxygen species; SILAC, Stable Isotope Labeling by Amino acids in Cell culture; TFA, trifluoracetic acid; UASb, unaffected siblings.

Received December 15, 2022, and in revised form, May 31, 2023
Published, MCPRO Papers in Press, June 22, 2023, https://doi.org/10.1016/j.mcpro.2023.100605

REFERENCES

1. Statland, J. M., McDermott, M. P., Heatwole, C., Martens, W. B., Pandya, S., van der Kooi, E. L., *et al*. (2013) Reevaluating measures of disease progression in facioscapulohumeral muscular dystrophy. *Neuromuscul. Disord.* **23**, 306–312
2. Lemmers, R. J., van der Vliet, P. J., Klooster, R., Sacconi, S., Camano, P., Dauwerse, J. G., *et al*. (2010) A unifying genetic model for facioscapulohumeral muscular dystrophy. *Science* **329**, 1650–1653
3. Rickard, A. M., Petek, L. M., and Miller, D. G. (2015) Endogenous DUX4 expression in FSHD myotubes is sufficient to cause cell death and disrupts RNA splicing and cell migration pathways. *Hum. Mol. Genet.* **24**, 5901–5914
4. Winokur, S. T., Chen, Y. W., Masny, P. S., Martin, J. H., Ehmsen, J. T., Tapscott, S. J., *et al*. (2003) Expression profiling of FSHD muscle supports a defect in specific stages of myogenic differentiation. *Hum. Mol. Genet.* **12**, 2895–2907
5. Winokur, S. T., Barrett, K., Martin, J. H., Forrester, J. R., Simon, M., Tawil, R., *et al*. (2003) Facioscapulohumeral muscular dystrophy (FSHD) myoblasts demonstrate increased susceptibility to oxidative stress. *Neuromuscul. Disord.* **13**, 322–333
6. Dmitriev, P., Bou Saada, Y., Dib, C., Ansseau, E., Barat, A., Hamade, A., *et al*. (2016) DUX4-induced constitutive DNA damage and oxidative stress contribute to aberrant differentiation of myoblasts from FSHD patients. *Free Radic. Biol. Med.* **99**, 244–258
7. Banerji, C. R. S., and Zammit, P. S. (2021) Pathomechanisms and biomarkers in facioscapulohumeral muscular dystrophy: roles of DUX4 and PAX7. *EMBO Mol. Med.* **13**, e13695
8. Heher, P., Ganassi, M., Weidinger, A., Engquist, E. N., Pruller, J., Nguyen, T. H., *et al*. (2022) Interplay between mitochondrial reactive oxygen species, oxidative stress and hypoxic adaptation in facioscapulohumeral muscular dystrophy: metabolic stress as potential therapeutic target. *Redox Biol.* **51**, 102251
9. Wallace, L. M., Garwick, S. E., Mei, W., Belayew, A., Coppee, F., Ladner, K. J., *et al*. (2011) DUX4, a candidate gene for facioscapulohumeral muscular dystrophy, causes p53-dependent myopathy *in vivo*. *Ann. Neurol.* **69**, 540–552
10. Rahimov, F., King, O. D., Leung, D. G., Bibat, G. M., Emerson, C. P., Jr., Kunkel, L. M., *et al*. (2012) Transcriptional profiling in facioscapulohumeral muscular dystrophy to identify candidate biomarkers. *Proc. Natl. Acad. Sci. U. S. A.* **109**, 16234–16239
11. Tupler, R., Perini, G., Pellegrino, M. A., and Green, M. R. (1999) Profound misregulation of muscle-specific gene expression in facioscapulohumeral muscular dystrophy. *Proc. Natl. Acad. Sci. U. S. A.* **96**, 12650–12654
12. Arashiro, P., Eisenberg, I., Kho, A. T., Cerqueira, A. M., Canovas, M., Silva, H. C., *et al*. (2009) Transcriptional regulation differs in affected facioscapulohumeral muscular dystrophy patients compared to asymptomatic related carriers. *Proc. Natl. Acad. Sci. U. S. A.* **106**, 6220–6225
13. Jagannathan, S., Ogata, Y., Gafken, P. R., Tapscott, S. J., and Bradley, R. K. (2019) Quantitative proteomics reveals key roles for post-transcriptional gene regulation in the molecular pathology of facioscapulohumeral muscular dystrophy. *Elife* **8**, e41740
14. Jagannathan, S., Shadle, S. C., Resnick, R., Snider, L., Tawil, R. N., van der Maarel, S. M., *et al*. (2016) Model systems of DUX4 expression recapitulate the transcriptional profile of FSHD cells. *Hum. Mol. Genet.* **25**, 4419–4431
15. Brennan, C. M., Hill, A. S., St Andre, M., Li, X., Madeti, V., Breitkopf, S., *et al*. (2022) DUX4 expression activates JNK and p38 MAP kinases in myoblasts. *Dis. Model. Mech.* **15**, dmm049516
16. Laoudj-Chenivesse, D., Carnac, G., Bisbal, C., Hugon, G., Bouillot, S., Desnuelle, C., *et al*. (2005) Increased levels of adenine nucleotide translocator 1 protein and response to oxidative stress are early events in facioscapulohumeral muscular dystrophy muscle. *J. Mol. Med. (Berl.)* **83**, 216–224
17. Celegato, B., Capitanio, D., Pescatori, M., Romualdi, C., Pacchioni, B., Cagnin, S., *et al*. (2006) Parallel protein and transcript profiles of FSHD patient muscles correlate to the D4Z4 arrangement and reveal a common impairment of slow to fast fibre differentiation and a general deregulation of MyoD-dependent genes. *Proteomics* **6**, 5303–5321
18. Tassin, A., Leroy, B., Laoudj-Chenivesse, D., Wauters, A., Vanderplanck, C., Le Bihan, M. C., *et al*. (2012) FSHD myotubes with different phenotypes exhibit distinct proteomes. *PLoS One* **7**, e51865
19. Barro, M., Carnac, G., Flavier, S., Mercier, J., Vassetzky, Y., and Laoudj-Chenivesse, D. (2010) Myoblasts from affected and non-affected FSHD muscles exhibit morphological differentiation defects. *J. Cell. Mol. Med.* **14**, 275–289
20. Corasolla Carregari, V., Monforte, M., Di Maio, G., Pieroni, L., Urbani, A., Ricci, E., *et al*. (2020) Proteomics of muscle microdialysates identifies potential circulating biomarkers in facioscapulohumeral muscular dystrophy. *Int. J. Mol. Sci.* **22**, 290
21. Homma, S., Chen, J. C., Rahimov, F., Beermann, M. L., Hanger, K., Bibat, G. M., *et al*. (2012) A unique library of myogenic cells from facioscapulohumeral muscular dystrophy subjects and unaffected relatives: family, disease and cell function. *Eur. J. Hum. Genet.* **20**, 404–410
22. Ganassi, M., Figeac, N., Reynaud, M., Ortuste Quiroga, H. P., and Zammit, P. S. (2022) Antagonism between DUX4 and DUX4c highlights a pathomechanism operating through β-catenin in facioscapulohumeral muscular dystrophy. *Front. Cell Dev. Biol.* https://doi.org/10.3389/fcell.2022.802573

23. Masteika, I. F., Sathya, A., Homma, S., Miller, B. M., Boyce, F. M., and Miller, J. B. (2022) Downstream events initiated by expression of FSHD-associated DUX4: studies of nucleocytoplasmic transport, gammaH2AX accumulation, and Bax/Bak-dependence. *Biol. Open* **11**, bio059145
24. Stadler, G., Rahimov, F., King, O. D., Chen, J. C., Robin, J. D., Wagner, K. R., *et al*. (2013) Telomere position effect regulates DUX4 in human facioscapulohumeral muscular dystrophy. *Nat. Struct. Mol. Biol.* **20**, 671–678
25. Jones, T. I., King, O. D., Himeda, C. L., Homma, S., Chen, J. C., Beermann, M. L., *et al*. (2015) Individual epigenetic status of the pathogenic D4Z4 macrosatellite correlates with disease in facioscapulohumeral muscular dystrophy. *Clin. Epigenetics* **7**, 37
26. Banerji, C. R., Panamarova, M., Pruller, J., Figeac, N., Hebaishi, H., Fidanis, E., *et al*. (2019) Dynamic transcriptomic analysis reveals suppression of PGC1 α/ERR α drives perturbed myogenesis in facioscapulohumeral muscular dystrophy. *Hum. Mol. Genet.* **28**, 1244–1259
27. Burniston, J. G. (2019) Investigating muscle protein turnover on a protein-by-protein basis using dynamic proteome profiling. In: *Omics Approaches to Understanding Muscle Biology*, Springer, New York, NY: 171–190
28. Holmes, W. E., Angel, T. E., Li, K. W., and Hellerstein, M. K. (2015) Dynamic proteomics: in vivo proteome-wide measurement of protein kinetics using metabolic labeling. *Methods Enzymol.* **561**, 219–276
29. Pandey, S. N., Khawaja, H., and Chen, Y. W. (2015) Culture conditions affect expression of DUX4 in FSHD myoblasts. *Molecules* **20**, 8304–8315
30. Lim, K. R. Q., Bittel, A., Maruyama, R., Echigoya, Y., Nguyen, Q., Huang, Y., *et al*. (2021) DUX4 transcript knockdown with antisense 2'-O-Methoxyethyl gapmers for the treatment of facioscapulohumeral muscular dystrophy. *Mol. Ther.* **29**, 848–858
31. Camera, D. M., Burniston, J. G., Pogson, M. A., Smiles, W. J., and Hawley, J. A. (2017) Dynamic proteome profiling of individual proteins in human skeletal muscle after a high-fat diet and resistance exercise. *FASEB J.* **31**, 5478–5494
32. Burniston, J. G., Connolly, J., Kainulainen, H., Britton, S. L., and Koch, L. G. (2014) Label-free profiling of skeletal muscle using high-definition mass spectrometry. *Proteomics* **14**, 2339–2344
33. Hesketh, S. J., Sutherland, H., Lisboa, P. J., Jarvis, J. C., and Burniston, J. G. (2020) Adaptation of rat fast-twitch muscle to endurance activity is underpinned by changes to protein degradation as well as protein synthesis. *FASEB J.* **34**, 10398–10417
34. Stansfield, B. N., Brown, A. D., Stewart, C. E., and Burniston, J. G. (2021) Dynamic profiling of protein mole synthesis rates during C2C12 myoblast differentiation. *Proteomics* **21**, e2000071
35. Dittwald, P., Claesen, J. R., Burzykowski, T., Valkenborg, D., and Gambin, A. (2013) BRAIN: a universal tool for high-throughput calculations of the isotopic distribution for mass spectrometry. *Anal. Chem.* **85**, 1991–1994
36. Price, J. C., Holmes, W. E., Li, K. W., Floreani, N. A., Neese, R. A., Turner, S. M., *et al*. (2012) Measurement of human plasma proteome dynamics with (2)H(2)O and liquid chromatography tandem mass spectrometry. *Anal. Biochem.* **420**, 73–83
37. Storey, J. D., and Tibshirani, R. (2003) Statistical significance for genome-wide studies. *Proc. Natl. Acad. Sci. U. S. A.* **100**, 9440–9445
38. Zhang, B., Kirov, S., and Snoddy, J. (2005) WebGestalt: an integrated system for exploring gene sets in various biological contexts. *Nucleic Acids Res.* **33**, W741–W748
39. Eden, E., Navon, R., Steinfeld, I., Lipson, D., and Yakhini, Z. (2009) GOrilla: a tool for discovery and visualization of enriched GO terms in ranked gene lists. *BMC Bioinformatics* **10**, 48
40. Eden, E., Lipson, D., Yogev, S., and Yakhini, Z. (2007) Discovering motifs in ranked lists of DNA sequences. *PLoS Comput. Biol.* **3**, e39
41. Benjamini, Y., and Hochberg, Y. (1995) Controlling the false discovery rate: a practical and powerful approach to multiple testing. *J. Roy. Stat. Soc. B* **57**, 289–300
42. Franceschini, A., Szklarczyk, D., Frankild, S., Kuhn, M., Simonovic, M., Roth, A., *et al*. (2013) STRING v9.1: protein-protein interaction networks, with increased coverage and integration. *Nucleic Acids Res.* **41**, 808–815
43. Shannon, P., Markiel, A., Ozier, O., Baliga, N. S., Wang, J. T., Ramage, D., *et al*. (2003) Cytoscape: a software environment for integrated models of biomolecular interaction networks. *Genome Res.* **13**, 2498–2504
44. Heberle, H., Meirelles, G. V., da Silva, F. R., Telles, G. P., and Minghim, R. (2015) InteractiVenn: a web-based tool for the analysis of sets through Venn diagrams. *BMC Bioinformatics* **16**, 1–7
45. Rath, S., Sharma, R., Gupta, R., Ast, T., Chan, C., Durham, T. J., *et al*. (2021) MitoCarta3.0: an updated mitochondrial proteome now with sub-organelle localization and pathway annotations. *Nucleic Acids Res.* **49**, D1541–D1547
46. Turki, A., Hayot, M., Carnac, G., Pillard, F., Passerieux, E., Bommart, S., *et al*. (2012) Functional muscle impairment in facioscapulohumeral muscular dystrophy is correlated with oxidative stress and mitochondrial dysfunction. *Free Radic. Biol. Med.* **53**, 1068–1079
47. Bou Saada, Y., Dib, C., Dmitriev, P., Hamade, A., Carnac, G., Laoudj-Chenivesse, D., *et al*. (2016) Facioscapulohumeral dystrophy myoblasts efficiently repair moderate levels of oxidative DNA damage. *Histochem. Cell Biol.* **145**, 475–483
48. Homma, S., Beermann, M. L., Boyce, F. M., and Miller, J. B. (2015) Expression of FSHD-related DUX4-FL alters proteostasis and induces TDP-43 aggregation. *Ann. Clin. Transl. Neurol.* **2**, 151–166
49. Kowaljow, V., Marcowycz, A., Ansseau, E., Conde, C. B., Sauvage, S., Mattéotti, C., *et al*. (2007) The DUX4 gene at the FSHD1A locus encodes a pro-apoptotic protein. *Neuromuscul. Disord.* **17**, 611–623
50. Liu, X., Kim, C. N., Yang, J., Jemmerson, R., and Wang, X. (1996) Induction of apoptotic program in cell-free extracts: requirement for dATP and cytochrome c. *Cell* **86**, 147–157
51. Sun, L., Liu, Y., Fremont, M., Schwarz, S., Siegmann, M., Matthies, R., *et al*. (1998) A novel 52 kDa protein induces apoptosis and concurrently activates c-Jun N-terminal kinase 1 (JNK1) in mouse C3H10T1/2 fibroblasts. *Gene* **208**, 157–166
52. Chintharlapalli, S. R., Jasti, M., Malladi, S., Parsa, K. V., Ballestero, R. P., and Gonzalez-Garcia, M. (2005) BMRP is a Bcl-2 binding protein that induces apoptosis. *J. Cell. Biochem.* **94**, 611–626
53. Yoo, Y. A., Kim, M. J., Park, J. K., Chung, Y. M., Lee, J. H., Chi, S. G., *et al*. (2005) Mitochondrial ribosomal protein L41 suppresses cell growth in association with p53 and p27Kip1. *Mol. Cell. Biol.* **25**, 6603–6616
54. Kim, M. J., Yoo, Y. A., Kim, H. J., Kang, S., Kim, Y. G., Kim, J. S., *et al*. (2005) Mitochondrial ribosomal protein L41 mediates serum starvation-induced cell-cycle arrest through an increase of p21(WAF1/CIP1). *Biochem. Biophys. Res. Commun.* **338**, 1179–1184
55. Banerji, C. R., Knopp, P., Moyle, L. A., Severini, S., Orrell, R. W., Teschendorff, A. E., *et al*. (2015) β-Catenin is central to DUX4-driven network rewiring in facioscapulohumeral muscular dystrophy. *J. R. Soc. Interface* **12**, 20140797
56. Timms, R. T., Zhang, Z., Rhee, D. Y., Harper, J. W., Koren, I., and Elledge, S. J. (2019) A glycine-specific N-degron pathway mediates the quality control of protein N-myristoylation. *Science* **365**, eaaw4912
57. Passerieux, E., Hayot, M., Jaussent, A., Carnac, G., Gouzi, F., Pillard, F., *et al*. (2015) Effects of vitamin C, vitamin E, zinc gluconate, and selenomethionine supplementation on muscle function and oxidative stress biomarkers in patients with facioscapulohumeral dystrophy: a double-blind randomized controlled clinical trial. *Free Radic. Biol. Med.* **81**, 158–169
58. Denny, A. P., and Heather, A. K. (2017) Are antioxidants a potential therapy for FSHD? a review of the literature. *Oxid. Med. Cell. Longev.* **2017**, 7020295
59. Bosnakovski, D., Choi, S. H., Strasser, J. M., Toso, E. A., Walters, M. A., and Kyba, M. (2014) High-throughput screening identifies inhibitors of DUX4-induced myoblast toxicity. *Skelet. Muscle* **4**, 4
60. Lei, H., and Kazlauskas, A. (2014) A reactive oxygen species-mediated, self-perpetuating loop persistently activates platelet-derived growth factor receptor alpha. *Mol. Cell. Biol.* **34**, 110–122
61. Welsby, I., Hutin, D., Gueydan, C., Kruys, V., Rongvaux, A., and Leo, O. (2014) PARP12, an interferon-stimulated gene involved in the control of protein translation and inflammation. *J. Biol. Chem.* **289**, 26642–26657
62. Vanderplanck, C., Ansseau, E., Charron, S., Stricwant, N., Tassin, A., Laoudj-Chenivesse, D., *et al*. (2011) The FSHD atrophic myotube phenotype is caused by DUX4 expression. *PLoS One* **6**, e26820
63. Geng, L. N., Yao, Z., Snider, L., Fong, A. P., Cech, J. N., Young, J. M., *et al*. (2012) DUX4 activates germline genes, retroelements, and immune mediators: implications for facioscapulohumeral dystrophy. *Dev. Cell* **22**, 38–51
64. Van Der Heide, L. P., Hoekman, M. F., and Smidt, M. P. (2004) The ins and outs of FoxO shuttling: mechanisms of FoxO translocation and transcriptional regulation. *Biochem. J.* **380**, 297–309

65. Nishimura, Y., Chunthorng-Orn, J., Lord, S., Musa, I., Dawson, P., Holm, L., *et al*. (2022) Ubiquitin E3 ligase Atrogin-1 protein is regulated via the rapamycin-sensitive mTOR-S6K1 signaling pathway in C2C12 muscle cells. *Am. J. Physiol. Cell Physiol.* **323**, C215–C225
66. Sandri, M., Sandri, C., Gilbert, A., Skurk, C., Calabria, E., Picard, A., *et al*. (2004) Foxo transcription factors induce the atrophy-related ubiquitin ligase atrogin-1 and cause skeletal muscle atrophy. *Cell* **117**, 399–412
67. Zhao, J., Brault, J. J., Schild, A., Cao, P., Sandri, M., Schiaffino, S., *et al*. (2007) FoxO3 coordinately activates protein degradation by the autophagic/lysosomal and proteasomal pathways in atrophying muscle cells. *Cell Metab.* **6**, 472–483
68. Mammucari, C., Milan, G., Romanello, V., Masiero, E., Rudolf, R., Del Piccolo, P., *et al*. (2007) FoxO3 controls autophagy in skeletal muscle *in vivo*. *Cell Metab.* **6**, 458–471
69. Hartl, F. U., and Hayer-Hartl, M. (2002) Molecular chaperones in the cytosol: from nascent chain to folded protein. *Science* **295**, 1852–1858
70. Bukau, B., Deuerling, E., Pfund, C., and Craig, E. A. (2000) Getting newly synthesized proteins into shape. *Cell* **101**, 119–122
71. Cambridge, S. B., Gnad, F., Nguyen, C., Bermejo, J. L., Kruger, M., and Mann, M. (2011) Systems-wide proteomic analysis in mammalian cells reveals conserved, functional protein turnover. *J. Proteome Res.* **10**, 5275–5284
72. Yao, Z., Snider, L., Balog, J., Lemmers, R. J., Van Der Maarel, S. M., Tawil, R., *et al*. (2014) DUX4-induced gene expression is the major molecular signature in FSHD skeletal muscle. *Hum. Mol. Genet.* **23**, 5342–5352
73. Klooster, R., Straasheijm, K., Shah, B., Sowden, J., Frants, R., Thornton, C., *et al*. (2009) Comprehensive expression analysis of FSHD candidate genes at the mRNA and protein level. *Eur. J. Hum. Genet.* **17**, 1615–1624
74. Gabellini, D., Green, M. R., and Tupler, R. (2002) Inappropriate gene activation in FSHD: a repressor complex binds a chromosomal repeat deleted in dystrophic muscle. *Cell* **110**, 339–348
75. Jones, T. I., Chew, G. L., Barraza-Flores, P., Schreier, S., Ramirez, M., Wuebbles, R. D., *et al*. (2020) Transgenic mice expressing tunable levels of DUX4 develop characteristic facioscapulohumeral muscular dystrophy-like pathophysiology ranging in severity. *Skelet. Muscle* **10**, 8
76. Perez-Riverol, Y., Csordas, A., Bai, J., Bernal-Llinares, M., Hewapathirana, S., Kundu, D. J., *et al*. (2019) The PRIDE database and related tools and resources in 2019: improving support for quantification data. *Nucleic Acids Res.* **47**, D442–D450